Viscosity and Porosity Contribute to both Speed and Decay of Tectorial Membrane Traveling Waves

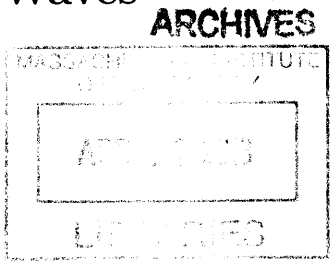

by

Jonathan Blake Sellon

S.B., University of Chicago (2010)

Submitted to the Department of Electrical Engineering and Computer Science
in partial fulfillment of the requirements for the degree of

Master of Science in Electrical Engineering and Computer Science

at the

MASSACHUSETTS INSTITUTE OF TECHNOLOGY

February 2013

Author .....
Department of Electrical Engineering and Computer Science
January 28, 2013

Certified by .....
Dennis M. Freeman
Professor of Electrical Engineering
Thesis Supervisor

Accepted by .....
Leslie A. Kolodziejski
Chairman, Department Committee on Graduate Theses

Viscosity and Porosity Contribute to both Speed and Decay of Tectorial Membrane Traveling Waves

by

Jonathan Blake Sellon

Submitted to the Department of Electrical Engineering and Computer Science
on January 28, 2013, in partial fulfillment of the
requirements for the degree of
Master of Science in Electrical Engineering and Computer Science

Abstract

The tectorial membrane (TM) is thought to play a critical role in stimulating cochlear hair cells. Recently, it has been shown that the tectorial membrane supports traveling waves [14] and that these waves may contribute to cochlear tuning and sensitivity by longitudinally coupling radial cross sections [15]. While previous work examined how TM wave properties may impact a variety of hearing properties, the molecular origins controlling wave propagation are still unclear. To better understand molecular mechanisms, I examined the role of porosity and viscosity in wave propagation. Wave properties were measured for mouse TMs immersed in artificial endolymph solutions with poly-ethylene glycol (PEG) added to increase viscosity. Two PEGs with different molecular weights (MW) were used: one (8 kDa) chosen to penetrate TM pores [30] while the other (400 kDa) could not. Findings show that introducing small MW PEG increases TM wave speeds by ~38% and decreases wave decay constants by ~42%. Analysis of a lumped parameter model of the TM showed that these changes in wave parameters can be explained by a change in shear viscosity from ~0.2 Pa*s to ~0.65 Pa*s with no accompanying change in shear modulus. In contrast, introducing large MW PEG has little effect on wave speed (~2%) or decay (~9%), suggesting shear viscosity inside the TM is significantly more important compared to fluid viscosity. This result suggests that fluid surrounding the TM has two separate effects on TM motion. First, increasing fluid viscosity has the obvious effect of increasing drag on the surface of the TM. In addition, if high viscosity fluid penetrates the TMs porous structure then the TMs material properties are also directly affected. Of these two effects, the latter has a much greater impact on TM waves. Thus, the porosity of the TM may play a critical role in cochlear mechanics.

Thesis Supervisor: Dennis M. Freeman
Title: Professor of Electrical Engineering

Acknowledgments

Several individuals have devoted an immense number of hours to help me grow as a scientist—this document would not have come to fruition without their help. First and foremost, I would like to thank my advisor Denny Freeman for pushing me to succeed and for playing a key role in helping me develop as an experimental researcher. Denny's rigor in thinking through each step of a problem while simultaneously understanding how the result fits into the field as a whole is not only refreshing, but has pushed me to become a better scientist. Having Denny as a mentor made the challenge of traversing into a new field enormously exciting and rewarding. I cannot thank him enough for the countless hours. Secondly, I want to thank my office mate Shirin Farrahi for all her help since I arrived at MIT. Shirin provided immeasurable support as I learned new experimental techniques and programming skills—I cannot thank her enough. Next, I want to thank my other fantastic lab mates Scott Page and Roozbeh Ghaffari. Scott's technical prowess in programming is astounding and it was fantastic to work with him over the past two years. Furthermore, Roozbeh's constant eye on the big picture and help throughout the project was enormously helpful not only for completion of this project, but for development as a scientist. Finally, I want to thank Salil Desai for his advice on navigating scientific problems and the politics of science itself. Interacting with Salil has been a pleasure and it has been fantastic to work with him over the past two years.

Beyond my lab, I also would like to thank my academic advisor Prof. John Guinan who has provided great advice since starting graduate school. Furthermore, I want to thank Profs. Charlie Liberman and Ruth Anne Eatock for their support and feedback as I have learned and explored more into how the auditory system functions.

I would also like to thank and acknowledge two funding sources that have allowed me to pursue the work presented here and the freedom to pursue new and exciting problems. Specifically, training grant support from the National Institute on Deafness and other Communication Disorders (NIDCD) and the National Science Foundation's (NSF) Graduate Research Fellowship Program (GRFP). Furthermore, I want to thank

my advisors who were instrumental in helping me receive this funding: Profs. Dennis Freeman, Margaret Gardel (University of Chicago, Chicago, IL), and Mordecai-Mark Mac Low (American Museum of Natural History, New York, NY).

In addition to having great lab mates and advisors, I also want to acknowledge my friends and program mates who were great supports throughout the entire process: Luke Shaheen, Goldie Mehraei, Jonathon Whitton, David Chaan, Samiya Alkhairy, Will Feng, Jesse Engreitz, Vikram Juneja, Brian Clark, Will McLean, Saul Glasman, Nicole Neubarth, Monica Thanawala, Carl Brozek, and Adam Anderson.

Finally, I want to thank those who were around from the beginning, before I ever set foot at MIT. My parents Lynn and Chris Sellon for dedicating their lives to helping me succeed over the past two and a half decades, my sister Lea Sellon for her playful demeanor and support, and my brother Dan Sellon for always questioning and being there for me. Without you, I would not have made it to this point today.

Contents

List of Figures

Chapter 1

Introduction

The cochlea is a remarkable sensor that is able to detect displacements on the order of magnitude of a hydrogen atom at frequencies up to 20,000 Hz in humans. This extraordinary sensitivity arises from a multitude of factors one of which being a collection of mechano-electrical receptors (hair cells) that reside along the cochlea's basilar membrane. While there has been an extensive body of research examining the basilar membrane and hair cells, there is much less known about the tectorial membrane. Given the tectorial membrane's location immediately above the cochlea's hair cells it is likely vital for transmission of acoustic signals. However, the extent and nature of the stimuli provided to hair cells via this membrane is currently unknown. Recently, a traveling wave mechansim [14] of the tectorial membrane has been identified and may influence a variety of mechanisms involved in cochlear sensitivity and selectivity. This thesis aims to uncover the molecular foundations of the tectorial membrane that allow for traveling waves and ultimately to shed light on the physiological role of the tectorial membrane in hearing. Specifically, this work examines the role of the TM's shear viscosity in supporting traveling waves.

1.1 The Mammalian Cochlea

Mammalian hearing is dependent on transmission of mechanical vibrations to the cochlea's inner hair cells. Hair cells are classified into two classes: inner (IHCs) and

outer hair cells (OHCs), each of which functions in a unique role. IHCs ultimately act as receptors that transmit signals to the brain via afferent nerve fibers while OHCs are predominantly innervated by efferent nerves originating from the brain. These OHCs trigger electromotility [3, 22] via prestin molecules so that sound stimuli can be amplified. Both types of hair cells contain densely packed arrays of stereocilia, each of which contains a mechanically sensitive transduction channel [21]. Above these hair bundles is an acellular matrix, the tectorial membrane (TM). The TM contacts the OHCs at their stereocilia [28] and sits above the IHC hair bundles (figure 1-1). Given the location of the TM, it is likely that it plays a vital role stimulating rows of inner and outer hair cells. Furthermore, given the notion that OHCs play a role in amplification via electromotility, it is very possible that they transmit mechanical signals back to the tectorial membrane for further amplification. By providing a mechanism for stimulation for inner and outer hair cells, the TM is an essential component of mammalian hearing.

1.2 TM Composition and Previous Measurements

The TM is known to be composed of collagen fibers (3% of total weight) that are held together via a porous matrix of highly charged glycosaminoglycans (GAGs). [12] To date, most TM measurements have been conducted on isolated samples removed from the cochlea. Previous work conducted *in vitro* demonstrated that the TM's mechanical properties change with frequency [1]. Furthermore, it is also known that the TM is stiffer in the radial direction compared to the longitudinal direction [18]. More recently, the isolated TM has also been shown [14] to support a traveling wave which has similar velocity to the traveling waves present on the basilar membrane. Given these properties, it is possible that these waves contribute to amplification, and ultimately the characteristic sensitivity and selectivity of mammalian hearing. Genetic models have also been created to verify the importance of the TM in maintaining proper tuning and sensitivity. For example, mutations in the TectB gene encoding β-tectorin revealed an interesting hearing phenotype [27, 26, 35, 34, 39]. Specifically,

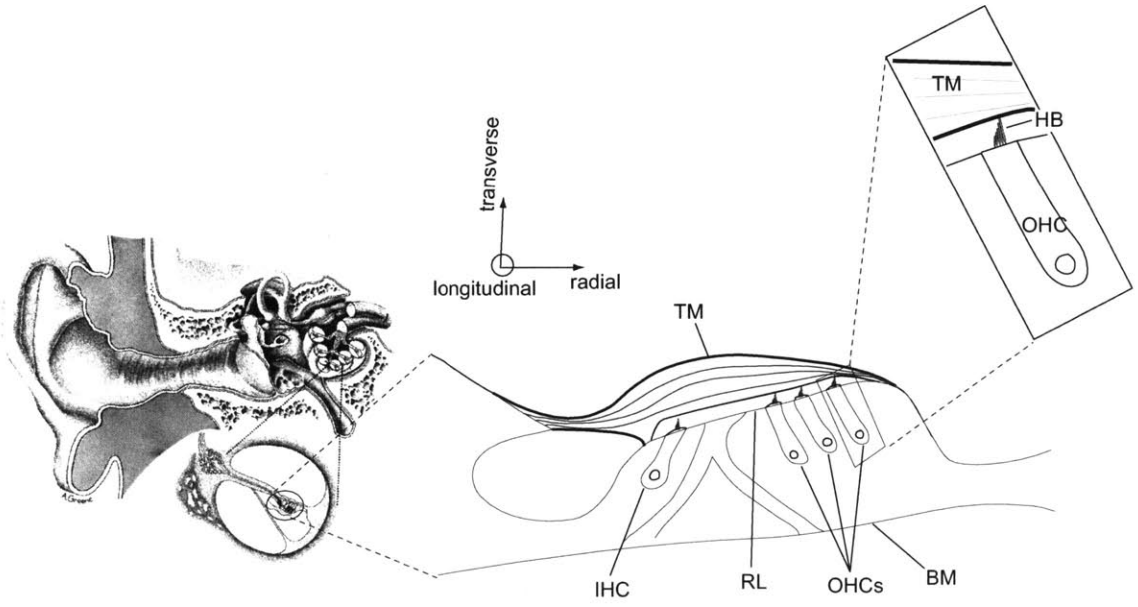

Figure 1-1: Left: Schematic of the cochlea, middle ear, and outer ear (drawing by Anne Greene). Middle: Schematic of the organ of Corti. On the apical surface, hair cells are seated in the reticular lamina (RL). Here, note that sensory hair cells (OHCs and IHC) lay underneath the tectorial membrane and sit on the basilar membrane (BM). The volume enclosed by the undersurface of the TM and the RL forms the subtectorial space. Right: The tips of OHC hair bundles (HB) contact the TM's bottom surface.

for the TectB mutation it was seen that mice had sharpened cochlear tuning in basal regions and elevated thresholds in apical regions. Further work has demonstrated that the traveling wave theory for TM motion can completely explain these hearing phenotypes [15].

While there is a large body of evidence that supports the importance of the TM to maintain normal cochlear function, little is known about how the TM's underlying dynamic molecular properties contribute to its mechanistic role in hearing. Classically, models describing the TM's role in hearing describe the membrane as a stiff lever with a compliant hinge and as a resonant mass-spring system. [8, 5, 32, 33, 2, 42, 29] However, these models assume that the TM is a static system and they neglect to explain recent findings such as longitudinal coupling [41, 15]. Given recent evidence that the TM is a poro-elastic tissue [30] and that it can support traveling waves [31, 15], it is highly probable that the underlying molecular properties are finally tuned to achieve proper tuning and sensitivity. Thus, this thesis explores the effect of porosity on TM waves by exploring the role of the TM's intrinsic viscosity.

1.3 Significance and Project Goals

The interdependence of mechanical, chemical, osmotic and electrical properties contribute to the TM's unique characteristics [23, 24, 25, 36, 10, 12]. Previous measurements have shown that even the smallest ionic changes in endolymphatic bath result in significant changes to the TM's dynamic properties [11, 12, 30], so there is reason to believe that they are tightly controlled in order to give rise to different hearing related properties. Thus, this thesis explores how the tectorial membrane's underlying poroelastic structure is responsible for maintaining proper cochlear function by focusing on the role of viscosity in TM wave propagation.

Poro-elastic materials have two properties that contribute to their dynamic nature: stiffness and viscosity. Previously it was reported that modulating stiffness impacted TM wave decay and thus could impact cochlear tuning. [9] Results from this work explain origins of sharpened tuning seen in mice lacking β-tectorin, but do not explain

changes in sensitivity observed in these mutant mice. Thus, this study focuses on the role of the other essential property of poro-elastic materials: viscosity. Specifically, this study addresses the impact of viscosity on longitudinal coupling of the TM via waves. By manipulating the viscosity within the TM, this thesis demonstrates that viscosity is essential for maintaining proper TM wave speed and wave decay. Finally, by appealing to a recent model examining the effect of tectorial membrane and basilar membrane longitudinal coupling [31], this thesis reveals how TM viscosity could play a critical role in maintaining proper cochlear sensitivity.

1.3.1 TM Pore Size and Intrinsic Viscosity

Recently, several poroelastic bulk properties of the tectorial membrane have been determined by exerting osmotic stress on the membrane. Specifically, the equilibrium stress-strain relation and the pore radius of mouse tectorial membrane were determined by exposing the membrane to polyethylene glycol (PEG) solutions of a range of molecular masses (20-511 kDa) [30]. In the study, it was inferred that for smaller molecular masses, PEG entered the TM and exerted a smaller effective osmotic pressure. Ultimately, the pore radius of the TM was estimated as 22nm.

Given that the pore radius of the mouse tectorial membrane is known, the first goal of this study was to change the internal viscosity of the TM without changing osmotic stress. By introducing small molecular mass PEG (8kDa) to the TM, this study reveals the effect of internal viscosity on TM dynamic properties. By examining how wave speed and decay change when adding small molecular weight PEGs to artificial endolymph surrounding the TM *in vitro*, this thesis reveals how TM dynamic properties are impacted by pore size. Next, by introducing PEGs of molecular weights larger than the pore size of the TM, this study reveals the importance of the intrinsic viscosity of the TM in contrast to the viscosity of the fluid surrounding the membrane.

1.3.2 Aims

To assess the importance of viscosity and porosity in controlling dynamic TM processes, this study examines:

(1) The effect of increasing the TM's internal viscosity via small molecular weight PEG on

- TM wave speed and decay constant
- Wave parameters of TectB mutant TMs
- Shear impedance of the TM
- Wave parameter predictions from shear impedance measurements
- Electrokinetic responses
- TM material properties determined from a distributed impedance model

(2) The effect of increasing the viscosity external to the TM's via large molecular weight PEG on

- TM wave speed and decay constant
- Electrokinetic responses

(3) How viscoelastic models of TM waves can predict the speed and decay constants found in this study

Ultimately, these measurements reveal how the poroelastic properties of the TM can impact dynamic properties of the TM such as traveling waves and influence properties of hearing.

Chapter 2

Methods

This chapter describes methods used to probe the importance of viscosity and porosity on dynamic function of the TM.

2.1 Isolated TM Preparation

TM segments were excised from adult mice (strain B6129F1, 4-12 weeks old, 1530 g; Jackson Lab, Bar Harbor, ME). TM segments were acquired by gently chipping the cochlea to expose the organ of Corti. Using a combination of dark and bright-field illumination, the TM was exposed and removed from the organ of Corti under a dissection microscope (Zeiss). Segments 0.5-1 mm in longitudinal length were isolated from the organ of Corti via a sterilized eyelash probe while in an artificial endolymph bath containing 174 mM KCl, 5 mM HEPES, 3 mM dextrose, 2 mM NaCl and 0.02 mM $CaCl_2$ in preparation for wave motion measurements. [14, 37] TM segments from high-frequency regions (1mm from the base) were classified 'basal' and those from low-frequency regions (1mm from the apex) were classified as 'apical' and used in this study. The bath used was titrated beforehand to pH 7.4 using KOH.

2.2 Measuring Solution Viscosities

To increase the shear viscosity of the TM, 8kDa PEG was added to the artificial endolymph (AE) solution (Sigma-Aldrich Inc., St. Louis, MO) at concentrations of 3mM, 10mM, and 20mM. To increase the viscosity around the TM, 2.5, 10, and 20 μM 400kDa polyethylene oxide (PEO) (Sigma-Aldrich Inc., St. Louis, MO) was added to the AE solution. The viscosities of the 3mM, 10mM, and 20mM PEG solutions were measured to be 1.3mPa*s, 3.4mPa*s, and 9.5mPa*s respectively via rheometry and a Cannon-Fenske viscometer (Technical Glass Products Inc., Dover, NH). The 2.5, 10, and 20μM 400kDa PEO solutions were measured to be 1.4mPa*s, 4.5mPa*s and 11 mPa*s respectively. Tables 1 (below) summarizes these measurements.

Concentration	8kDa PEG Viscosity	Concentration	400kDa PEO Viscosity
3mM	1.3mPa*s	2.5μM	1.4mPa*s
10mM	3.4mPa*s	10μM	4.5mPa*s
20mM	9.5mPa*s	20μM	11mPa*s

Table 1: Viscosities of 8kDa PEG and 400kDa PEO solutions

2.3 Launching Shear Waves on Isolated TM Segments

Isolated TM segments from the basal turn of mouse cochleae were suspended between the supports of a wave chamber [14] (figure 2-1). One of these supports was stationary while the other was attached with epoxy to a piezo-electric actuator (Thorlabs) and loosely coupled to the underlying glass slide with Vaseline. Before each experiment, motion of the vibrating support was examined to ensure uniform sinusoidal motion. To create a surface for the TM to adhere to within the chamber, the surface of the supports was coated with $\sim$0.2 μl of tissue adhesive (Cell Tak; Collaborative Research). Artificial endolymph solution was then perfused into the area between the supports and over the adhesive. The isolated TM was then injected into this medium

and mounted between the supports such that the TMs radial fibers were parallel to the vibrating support motion. Once mounted, the suspended TM was imaged with a transmitted-light microscope. Measurements were taken at physiological conditions (artificial endolymph) and then the medium was replaced with an artificial endolymph that included several concentrations of 8kDa PEG (3mM, 10mM, and 20mM) (figure 3-1a,c). The solutions were exchanged until the total volume (5mL) was replaced four times. The bath including PEG was then left for 10 minutes before performing measurements with the increased viscosity. Care was taken to ensure that the TM remained hydrated by keeping a small amount of the previous transfer over the TM. After observing waves in the presence of PEG the bath was returned to physiologic conditions with the same exchange procedure described and waves were measured again. This step was done to verify that the changes in wave parameters seen were due to changes in internal viscosity rather than time dependent effects. Once the exchange was complete, motions were recorded again. Using different TMs, this process was repeated with high molecular weight (400kDa) PEO at a concentration of 20μM, matching the viscosity of the 20mM 8kDa PEG.

2.4 Microfabricated Shear Impedance Probe

Shear impedance of the TM was obtained via microfabricated probes [18]. These probes were custom-designed with a range of stiffness values via a commercial MEMS foundry (MEMSCAP). Using tissue adhesive (Cell Tak, Collaborative Research) the probes were placed in contact with the surface of the TM (figure 2-2). Next, these probes were mechanically driven via a piezo-electric actuator (Thorlabs) at audio frequencies. Resulting measurements of the TM and the probe were determined with nanometer resolution from the images. After obtaining motions at physiological conditions PEG at a variety of concentrations (3mM, 10mM, and 20mM 8kDa) was introduced to the fluid surrounding the TM. When moving between concentrations, the solutions were exchanged until the total volume (5mL) was replaced four times. Once measurements at higher viscosities were complete, the bath was returned to

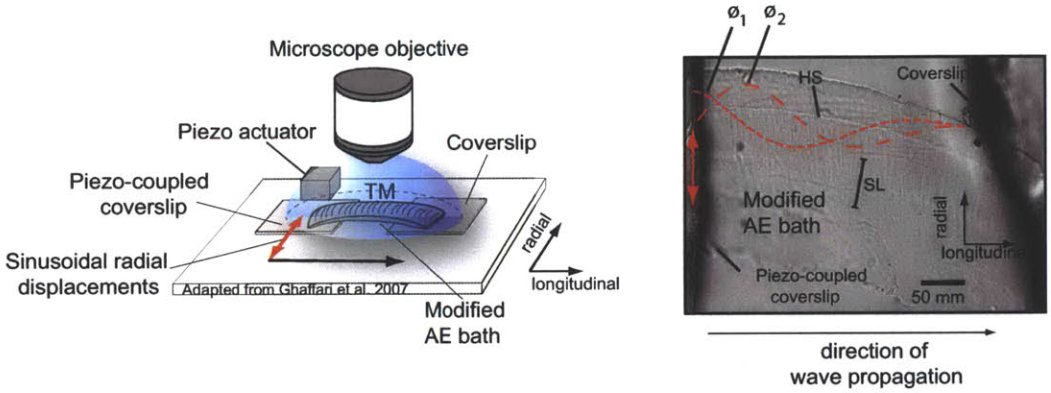

Figure 2-1: Schematic of the TM preparation in a wave chamber based on Ghaffari et al. 2007. Left: TM segment suspended between two coverslips separated by ~450 μm. This creates a free–floating region that can be visualized by a water immersion objective. Here, note that the piezo actuator is coupled to one coverslip to in order to generate radial displacements of the TM. Wave measurement are collected with a TM in artificial endolymph (AE) before and after introducing PEG to the bath. Right: Describes sinusoidal displacements applied to the TM. Important anatomical considerations include Hensen's stripe (HS) and the spiral limbus attachment (SL) as marked. Lines indicate TM motion at two sequential instances in time separated in phase by 90°. Motion magnification has been applied to demonstrate the wave–like nature of the motion.

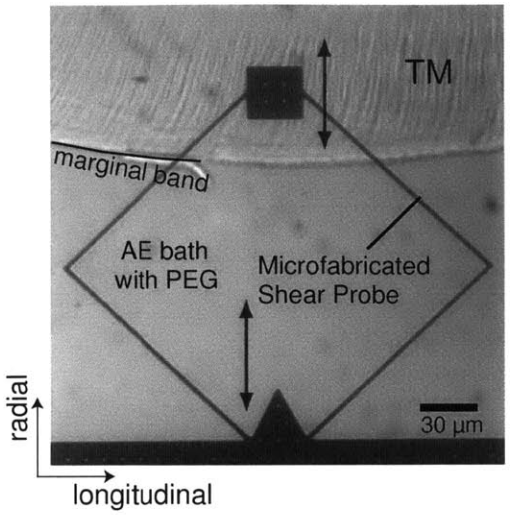

Figure 2-2: Microfabricated shearing probe applying forces in the radial and longitudinal directions. Shear measurement are collected with a TM in artificial endolymph (AE) before and after adding PEG to the solution.

physiologic conditions using artificial endolymph without PEG. This step was done to verify that the changes in shear impedance seen were due to changes in internal viscosity rather than time dependent effects. Once the exchange was complete, motions were recorded again. This shear impedance setup provided a way to probe TM dynamic properties with applied forces and displacements relevant to hearing.

2.5 Electrokinetic Measurements

Electrically-evoked radial displacements of the TM were evaluated via a microchannel chamber that delivered uniform electric fields [13]. This chamber involved an optically transparent PDMS channel that laid on a sheet of glass with Ag/AgCl stimulating electrodes (A-M Systems, WA), each of which was placed at one of the channel's two ends. The channel's glass surface was coated with $\sim 0.3\mu$L of Cell-Tak (BD Biosciences, MA) to allow the TM to adhere to the slide. A TM segment was then attached to the glass surface followed by placement of the PDMS channel over the TM. This process created a sealed channel that could be perfused with AE. Care was taken to orient the TM's radial fibers perpendicular to the direction of the applied

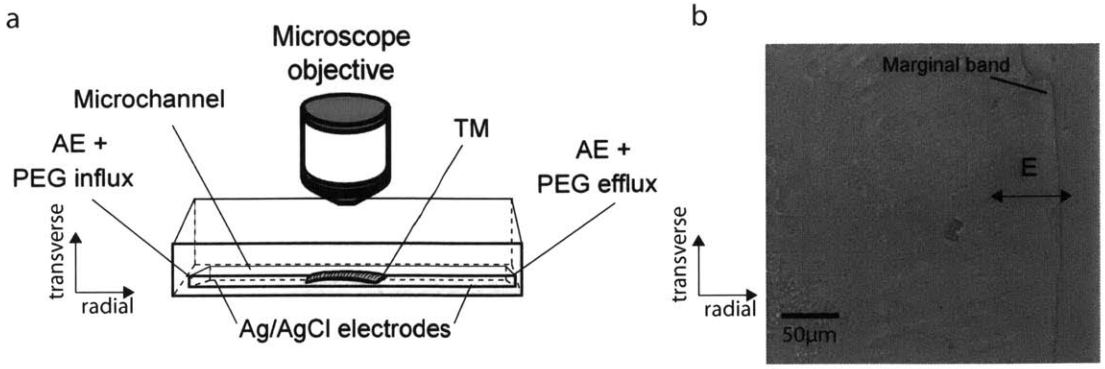

Figure 2-3: Microchannel setup with uniform electric fields applied radially to excised TM segments. (A) The TM was positioned between two application electrodes in microchannel. Electric fields were applied at audio frequencies with stroboscopic illumination and observed optically. (B) Light microscopy image of a TM segment in the microfluidics chamber. After obtaining a measurement in artificial endolymph, PEG of low molecular weight (10mM 8kDa) was added to the bath. After this measurement, AE without PEG was perfused and another measurement taken followed by another measurement with high molecular weight PEO (10μm 400kDa). The motion due to the applied field is highlighted with arrows just left of the marginal band.

electric field (figure 2-3). To assess the impact of pore size on electrokinetic motions, viscosity of the fluid inside and outside the TM was altered with PEG. TM motion measurements were first conducted in AE followed by AE with small molecular weight PEG (10mM, 8 kDa). After conducting this measurement the AE solution was brought back to physiologic conditions and TM motions were assessed again. Finally, AE with large molecular weight PEG (10 μL, 400 kDa) was added and TM motions were assessed, followed by another washout of PEG to test reversibility. Each of these solutions was perfused for 15 minutes so the TM could equilibrate prior to any motion measurement.

2.6 Stroboscopic Video Microscopy

The optical imaging system consisted of x20 water immersion objective with a 0.5 numerical aperture (for waves), a x40 water immersion objective with a 0.75 numerical aperture (for shear impedance) (Zeiss Axioplan) and a transmitted-light condenser

(0.8 numerical aperture). Images were captured with an 8 megapixel CCD camera (Stingray, Allied Vision Technologies, Germany) during stroboscopic illumination. To capture motions at audio frequencies, the stimuli (piezo-electric support for waves, micro fabricated probe for the shearing studies, and voltage changes for the electrokinetics studies) were timed with the stroboscopically pulsed LED light source with the frequency of stimulation. To reconstruct the wave motions, the TM was illuminated and images are captured at 8 evenly spaced stimulus phases over several stimulus cycles. Once obtained, the images were analyzed to determine the first three harmonics of motion.

2.6.1 Motion Analysis

From these images, magnitude and phase of radial displacement were computed from spatial and temporal brightness gradients [7]. Using computer vision algorithms, the magnitude and phase of displacements seen on the TM were computed from the series of images collected. These algorithms follow two assumptions: 1) the brightness of an object in the field of view is constant regardless of its position or time and 2) the object in the image being tracked moves as a rigid body.

Therefore,

$$\frac{\partial E}{\partial x}\Delta x + \frac{\partial E}{\partial y}\Delta y + \frac{\partial E}{\partial z}\Delta z + \frac{\partial E}{\partial t}\Delta t = 0, \tag{2.1}$$

where $E(x, y, z, t)$ is the brightness, which is shift invariant based on the first assumption [6, 7, 38].

2.6.2 Calculating Wave Parameters

Radial displacement and phase of the TM were determined from a one-dimensional FFT taken at evenly spaced regions of interest along the TM. Speeds, ?, were determined by fitting a linear regression to the phase. Wave speed was then calculated by taking the inverse slope of the phase versus distance and multiplying by frequency. Decay constants, σ, were defined as the distance along the TM over which the wave

magnitude decayed by a factor of e. These values were determined by fitting an exponential to the overall magnitude of the response along the TM.

2.7 Animal Preparation

Mice or gerbils were euthanized via carbon dioxide asphyxiation and decapitation immediately followed euthanasia. Tissue harvesting was performed as outlined in the previous section. The care and use of animals in this study were approved by the Massachusetts Institute of Technology Committee on Animal Care.

Chapter 3

Results

3.1 Tectorial Membrane Waves

Recently, waves have been shown to propagate longitudinally along the length of the tectorial membrane [14] and these waves have been characterized by their speed and decay. While these wave parameters have been characterized, it is unclear how the TM's molecular underpinnings control these waves. In this section, the role of viscosity and porosity in controlling was investigated by introducing PEG's of various sizes to the artificial endolymph solution surrounding the TM on the wave chamber (figure 3-1). Previously, PEG had been used to uncover the pore size of the TM [30], so PEGs of small molecular weights (8kDa) were used to modulate the internal viscosity of the TM and large molecular weight poly-ethylene oxide (PEO, 400kDa) was used to modulate the viscosity around the TM. Once wave motion images were obtained, two parameters were determined that describe wave properties—the wavelength, λ, which is how far the wave travels while going through a complete motion cycle, and wave decay constant, σ, the distance traveled before the wave amplitude dissipates by a factor of e. To obtain the wave speed parameter, change in phase a function of distance was examined while σ values involved fitting an exponential to the overall magnitude of the response along the length of the TM. Figure 3-1 and 3-2 demonstrate these fits to the raw data obtained for a TM in AE, AE with 8kDa PEG, and AE with 400kDa PEO.

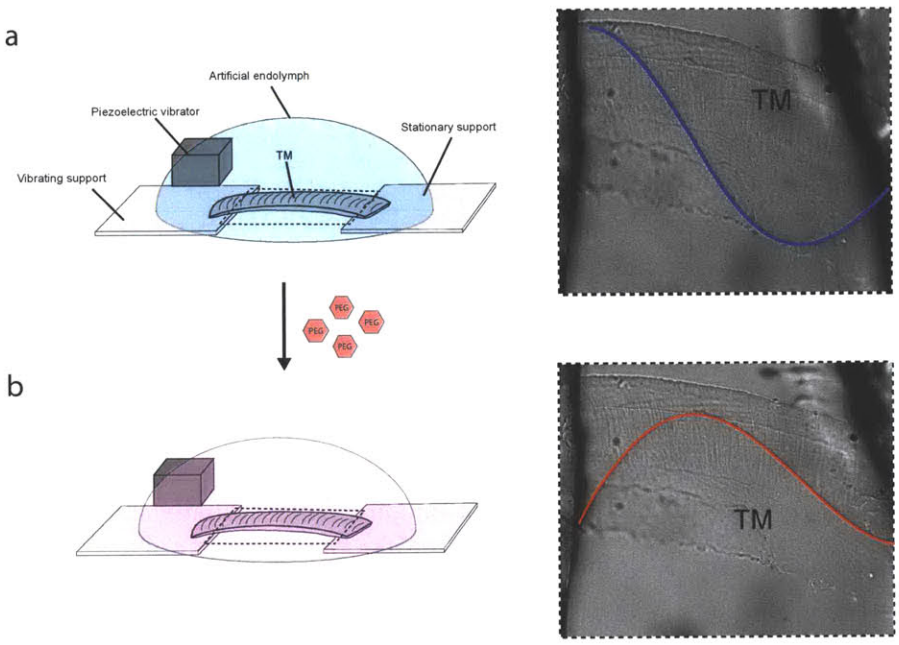

Figure 3-1: TM wave measurements with viscosity manipulations. (a) Left: Schematic depicting wave chamber setup. TM segments were suspended between two supports separated by ~400 μm and surrounded by artificial endolymph. One of these supports was vibrated at audio frequencies to transmit sinusoidal forces to the TM. Right: Light microscope image of a TM in artificial endolymph depicting wave motion in response to 19-kHz stimulation. Wave decay constant (σ) and speed (ν) were measured by fitting the decaying waves measured along the TM [14]. Best fitting wave parameter estimates were σ = ~380 μm and λ= ~130 μm for wild-type mice. (b) Left: Schematic depicting change to wave chamber setup to increase TM viscosity. After collecting images with artificial endolymph, 20mM 8kDa PEG was added to the bath surrounding the TM to alter the intrinsic viscosity of the TM. Right: Light microscope image of the same TM in artificial endolymph with PEG depicting wave motion in response to 19-kHz stimulation. Best fitting wave parameter estimates were σ = ~130 μm and λ= ~240 μm for this TM immersed in artificial endolymph with PEG.

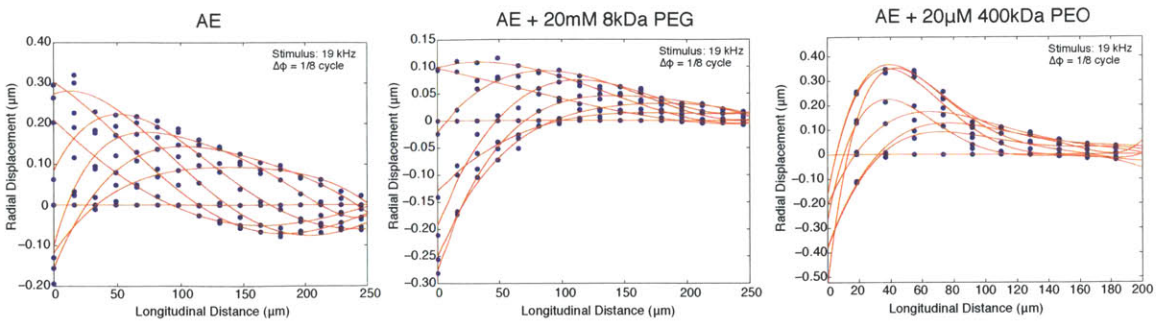

Figure 3-2: Radial displacements as a function of longitudinal distance for a single TM in AE (Left) and AE + 8kDa PEG (Middle). Another TM was introduced to 400kDa PEO (Right). Fits to eight phases of wave motion are presented.

3.1.1 Wave Properties and Intrinsic Viscosity

Wave Speeds

Eight phases of radial motion were captured before and after the introduction of PEG to TM segments (figure 3-1). The raw displacements shown in figure 3-1 were taken at stimulus frequencies of 19 kHz. This TM segment was isolated from the middle to the basal third of the cochlea and the waveform presented longer wavelengths with addition of PEG. Specifically, addition of 20mM 8kDa PEG had the effect of increasing the wavelength by nearly 85% in this instance. By pooling across frequencies (1-25kHz) and many basal segments, this trend manifests as increased wave speed at every frequency (figure 3-3a,b). Specifically, speeds were higher by a factor of $\sim$45%$\pm$35% when pooling across 5 TM's and all frequencies. This effect was also examined in apical segments and the same trend was seen (figure 3-4a,b). When PEG was added to the bath surrounding apical TM's wave speed increased by a factor of $\sim$45%$\pm$66%. These speed increases were also found to be reversible when the bath surrounding the TM was returned to back to physiological conditions (figure 3-8a). Wave speed differed by only $\sim$2%$\pm$22% between the initial measurement in AE and when the bath was returned to physiologic conditions.

In addition to adjusting TM viscosity with 20mM 8kDa PEG, other PEG concentrations were used to achieve different TM viscosities. A single TM was introduced

to solutions of increasing viscosity from 1.0 (AE) to 1.3 (AE + 3mM 8kDa PEG) 3.4 (AE + 10mM 8kDa PEG) to 9.5mPa*s (AE + 20mM 8kDa PEG). Upon ramping the viscosity of the AE solution with PEG, wave speed was seen to increase up to a point (figure 3-5). When increasing the viscosity of the AE solution beyond 3.4mPa*s, wave speed remained nearly the same.

Wave Decay Constants

In addition to changes in wave speed, wave decay was also seen to change when increasing bath viscosity from 1.0mPa*s to 9.5mPa*s via PEG. Pooling across 5 TM's revealed that increasing viscosity had the effect of decreasing wave decay constant in basal TM segments by a factor of 42%±30% (figure 3-6a,b). This effect was also seen for apical segments (figure 3-7a,b). Specifically, decay constant was seen to drop by a factor of 43%±25% in these apical segments. As with changes in speed, the change in decay constant was seen to be reversible. When removing PEG from the artificial endolymph bath (figure 3-8b) wave decay constants were seen to return to within 7%±33% of the decay constants observed at physiologic conditions.

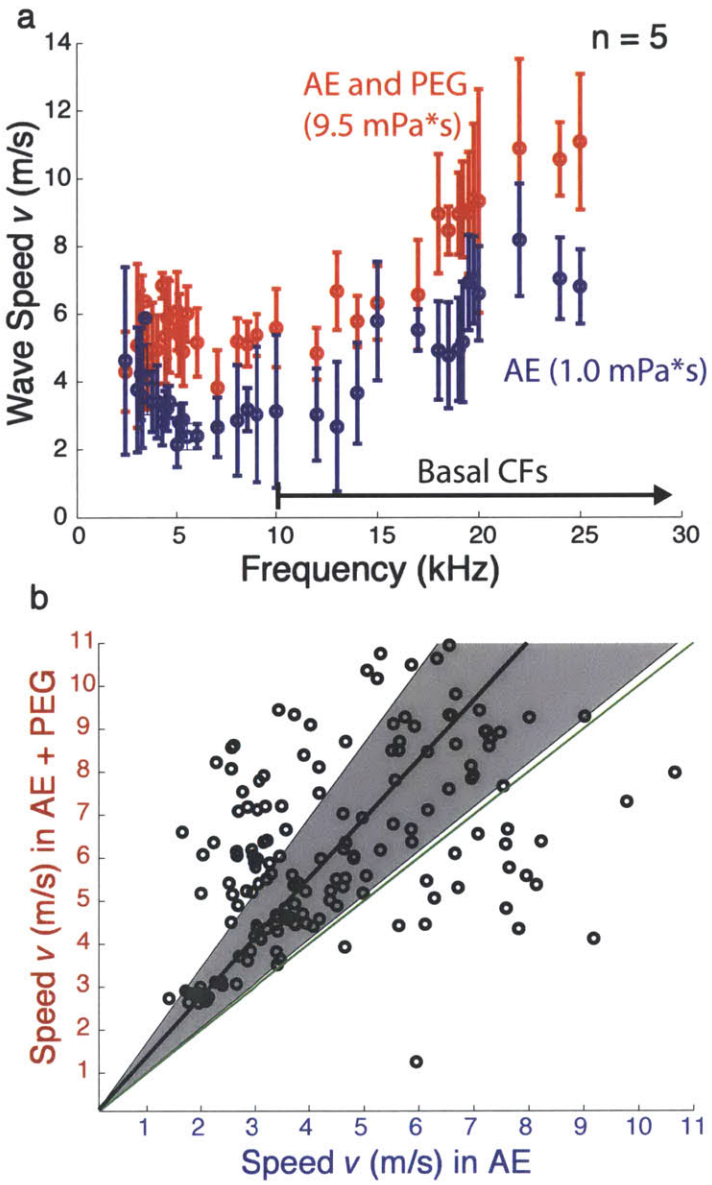

Figure 3-3: Dependance of propagation velocity of basal TM waves on viscosity. Median wave velocities and interquartile ranges measured in TMs immersed in artificial endolymph (blue circles) and artificial endolymph with PEG (red circles) at variety of stimulus frequencies. (a) The median velocities for basal TMs immersed in artificial endolymph with PEG were significantly higher (6.35 $\pm$ 2.01 m/s; n = 5 preparations) than those in just artificial endolymph (4.67 $\pm$ 1.99 m/s; n = 5 preparations). (b) Pairing the results with artificial endolymph speeds (x-axis) versus artificial endolymph (y-axis) also reveals the changes in speed. Median and interquartile ranges are indicated by black lines and shaded regions, respectively. ($\frac{v_{AE+PEG}}{v_{AE}} = 1.38 \pm 0.35$)

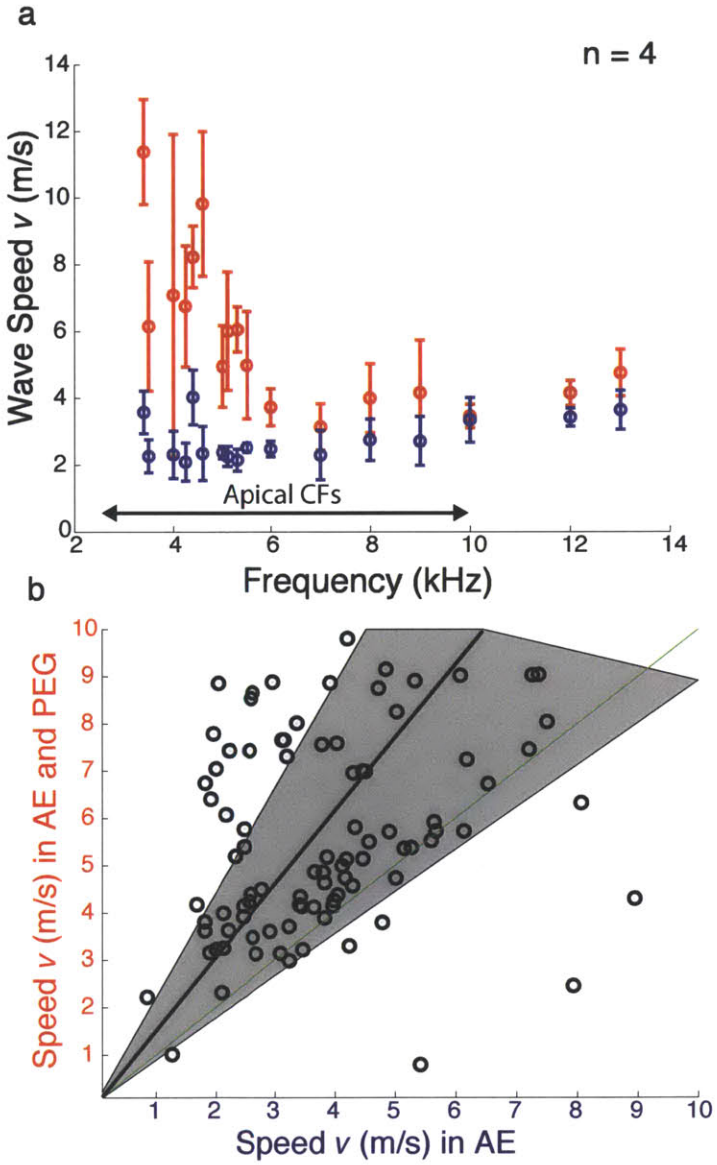

Figure 3-4: Propagation velocity of apical TM waves upon with increased viscosity. Median wave velocities and interquartile ranges measured in TMs immersed in artificial endolymph (blue circles) and artificial endolymph with PEG (red circles) at variety of stimulus frequencies. (a) The median velocities for apical TMs immersed in artificial endolymph with PEG were significantly higher (5.72 $\pm$ 2.05 m/s; n = 4 preparations) than those in just artificial endolymph (3.82 $\pm$ 1.15 m/s; n = 4 preparations). (b) Pairing the results with artificial endolymph speeds (x-axis) versus artificial endolymph with PEG (y-axis) also reveals the changes in speed. Median and interquartile ranges are indicated by black lines and shaded regions, respectively. ($\frac{v_{AE+PEG}}{v_{AE}} = 1.55 \pm 0.66$)

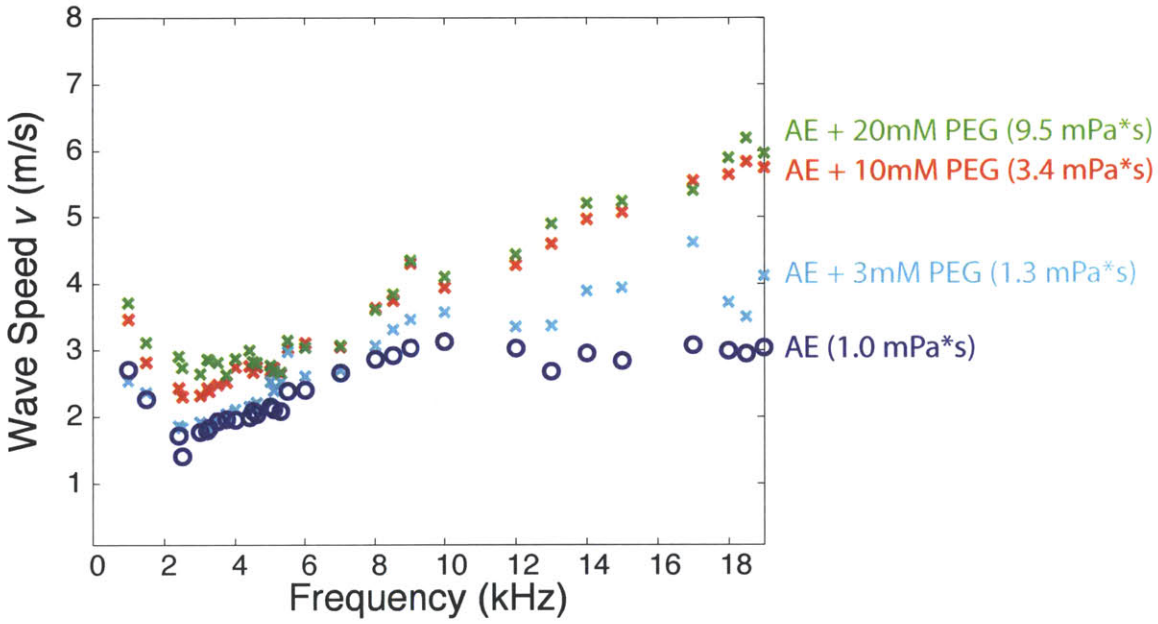

Figure 3-5: Basal TM wave measurements at physiological conditions (blue) vs artificial endolymph with 3mM 8kDa PEG (light blue), 10mM 8kDa PEG (red), 20mM 8kDa PEG (green). Each point represents a single frequency measurement on a single TM at physiological then increased viscosity conditions where stimuli were applied from 1-20 kHz via a piezo-electric vibrator.

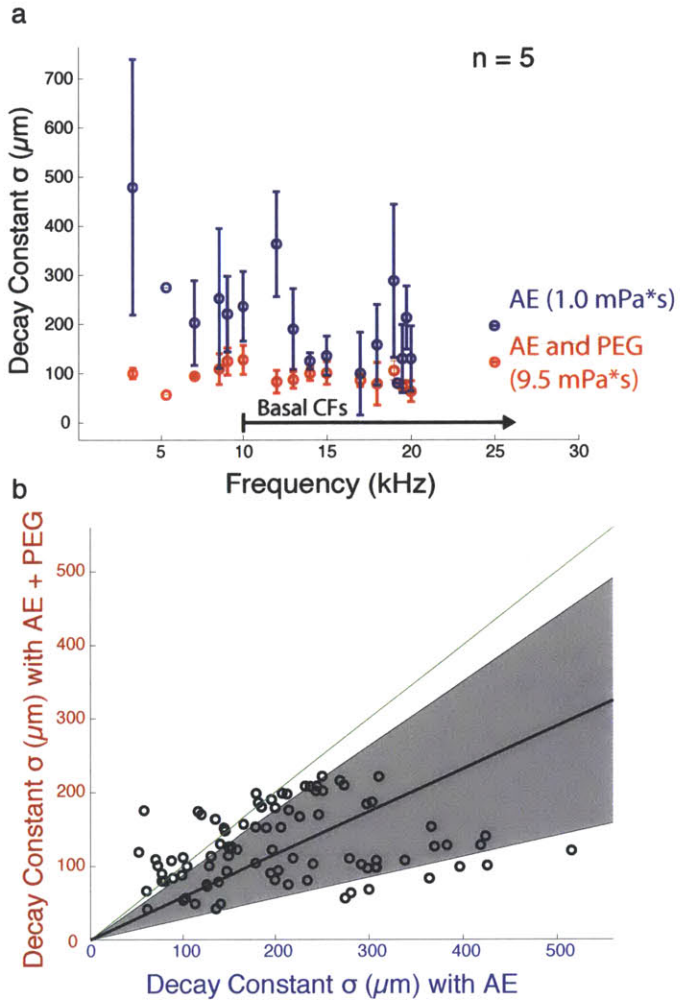

Figure 3-6: Wave decay constant calculation for basal TMs in artificial endolymph solutions with and without PEG. (a) Wave decay constants versus stimulus frequency. TM segments in artificial endolymph (n = 5 preparations, blue circles) had median wave decay constant (σ) values of 195 $\pm$ 69 μm. Introducing 8kDa PEG to the artificial endolymph solution (n = 5 preparations, red circles) had the effect of dropping these decay constants as they displayed median decay constants of 112 $\pm$ 41 μm for the same frequency range. (b) Pairing the data reveals the same trend of decreasing decay constant with increased viscosity. Wave parameters plotted with artificial endolymph (x-axis) and artificial endolymph with PEG (y-axis) (n = 5). Median and interquartile ranges are indicated by black lines and shaded regions, respectively. ($\frac{\sigma_{AE+PEG}}{\sigma_{AE}} = 0.58 \pm 0.30$).

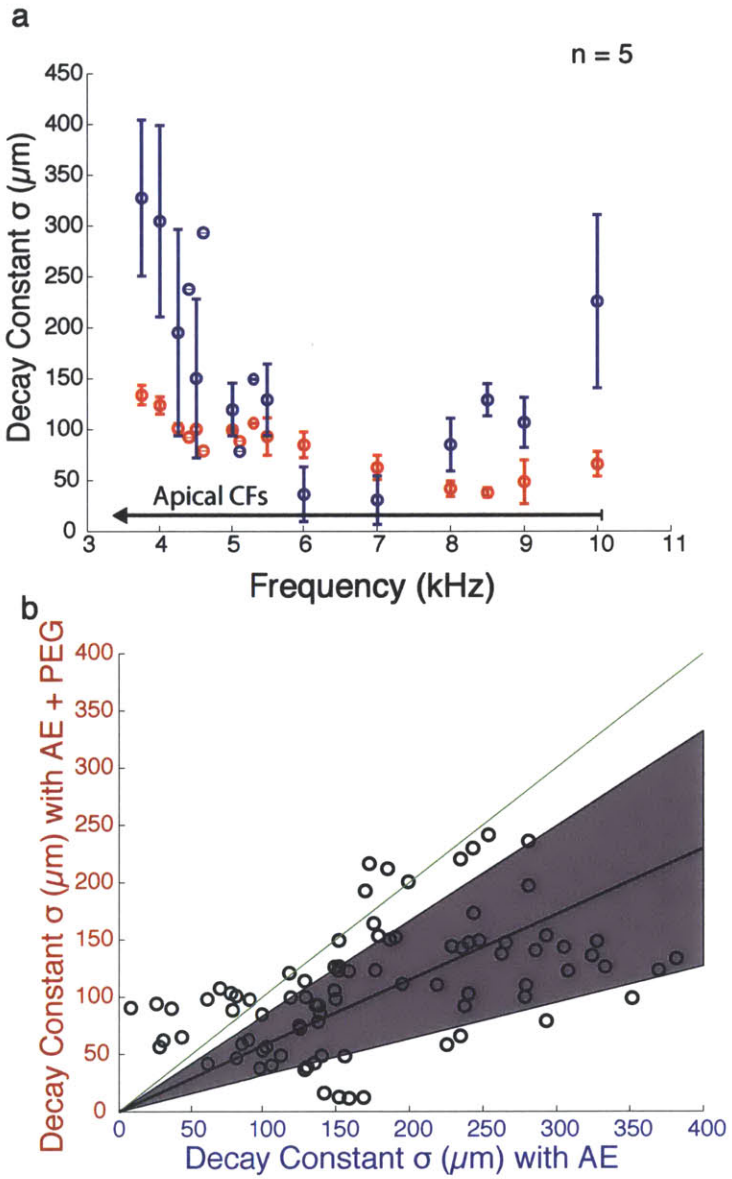

Figure 3-7: Wave decay constant calculation for apical TMs in artificial endolymph solutions with and without PEG. (a) Wave decay constants versus stimulus frequency. TM segments in artificial endolymph (n = 5 preparations, blue circles) had median wave decay constant (σ) values of 156 $\pm$ 61 μm. Introducing 8kDa PEG to the artificial endolymph solution (n = 5 preparations, red circles) had the effect of dropping these decay constants as they displayed median decay constants of 111 $\pm$ 36 μm for the same frequency range. (b) Pairing the data reveals the same trend of decreasing decay constant with increased viscosity. Wave parameters plotted with artificial endolymph (x-axis) and artificial endolymph with PEG (y-axis) (n = 5). Median and interquartile ranges are indicated by black lines and shaded regions, respectively. ($\frac{\sigma_{AE+PEG}}{\sigma_{AE}} = 0.57 \pm 0.25$).

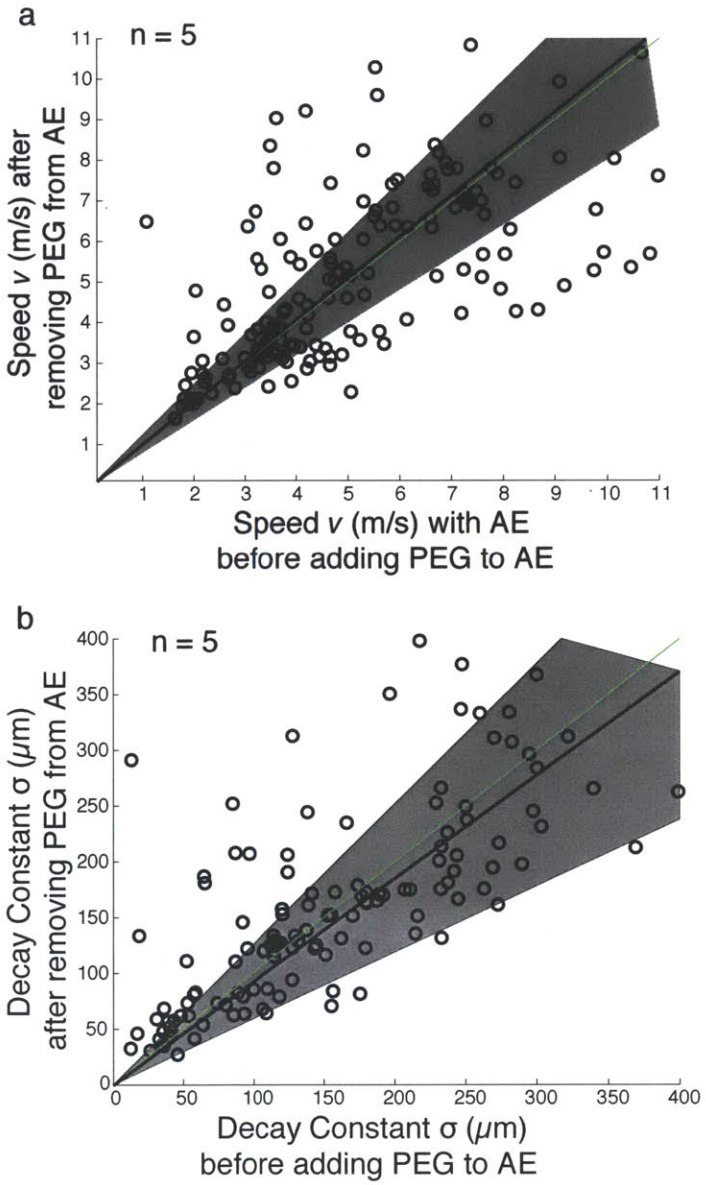

Figure 3-8: Propagation velocity and decay constants for basal TM waves before adding PEG to the AE solution and after removing PEG from the AE solutions. Result demonstrates that the effect of increasing TM viscosity can be reversed by replacing the AE+PEG bath with a bath just containing AE. (a) Velocities for basal TMs immersed in artificial endolymph before introducing PEG and after removing it were approximately the same. Here the data is paired (median and interquartile ranges indicated by black lines and shaded regions, respectively). ($\frac{v_{AEremovingPEG}}{v_{AEbeforePEG}} = 1.02 \pm 0.22$; n = 5 preparations) (b) Pairing decay constants reveals that decay also returns to normal when washing PEG out of the solution $\frac{\sigma_{AEremovingPEG}}{\sigma_{AEbeforePEG}} = 0.93 \pm 0.33$; n = 5 preparations).

3.1.2 Wave Properties and External Viscosity

In order to probe how the fluid around the TM impacts waves compared to the TM's intrinsic viscosity, this section involved examining the role of viscosity external to the TM and how it might affect wave parameters. Given that the pore size of the TM is known [30], it was possible to use poly-ethylene oxides (PEOs) of large molecular weights that could not penetrate the tectorial membrane. By introducing these large molecular weight PEOs (400 kDa), the viscosity outside the TM was increased, while the viscosity inside the TM was kept the same. PEO at 10 μM, 400kDa was used because it has a viscosity of 11 mPa*s, which approximately matches the viscosity of the 20mM 8kDa PEG used for the intrinsic viscosity study. By matching the viscosities it was possible to separate the effects of altering viscosity within the TM versus outside the TM. Surprisingly, introducing large MW PEG has little effect on wave speed (~2%) (figure 3-9) or decay (~9%) (figure 3-10), suggesting shear viscosity inside the TM is significantly more important than the viscosity outside of the TM.

3.2 Determining Material Properties from Waves

The wave properties observed on the TM are frequency dependent and yield information about the underlying material properties. For example, we can learn about the density ρ, the shear storage modulus G', and the shear viscosity η. G' describes the elastic energy stored when a body is deformed while η describes the dissipation of energy stored. The velocity, v, of pure shear waves in a viscoelastic material that is infinite and isotropic depend on these parameters as follows:

$$v = \sqrt{\frac{2(G'^2 + \omega^2\eta^2)}{\rho(\sqrt{G'^2 + \omega^2\eta^2}} \tag{3.1}$$

where ω is the angular frequency of vibration. [15, 4, 31] Using this distributed impedance model of TM waves, material properties of the TM were estimated by finding the values of G' and η that best fit the values of v measured with and without addition of PEG to the artificial endolymph. Since a wave chamber was used that

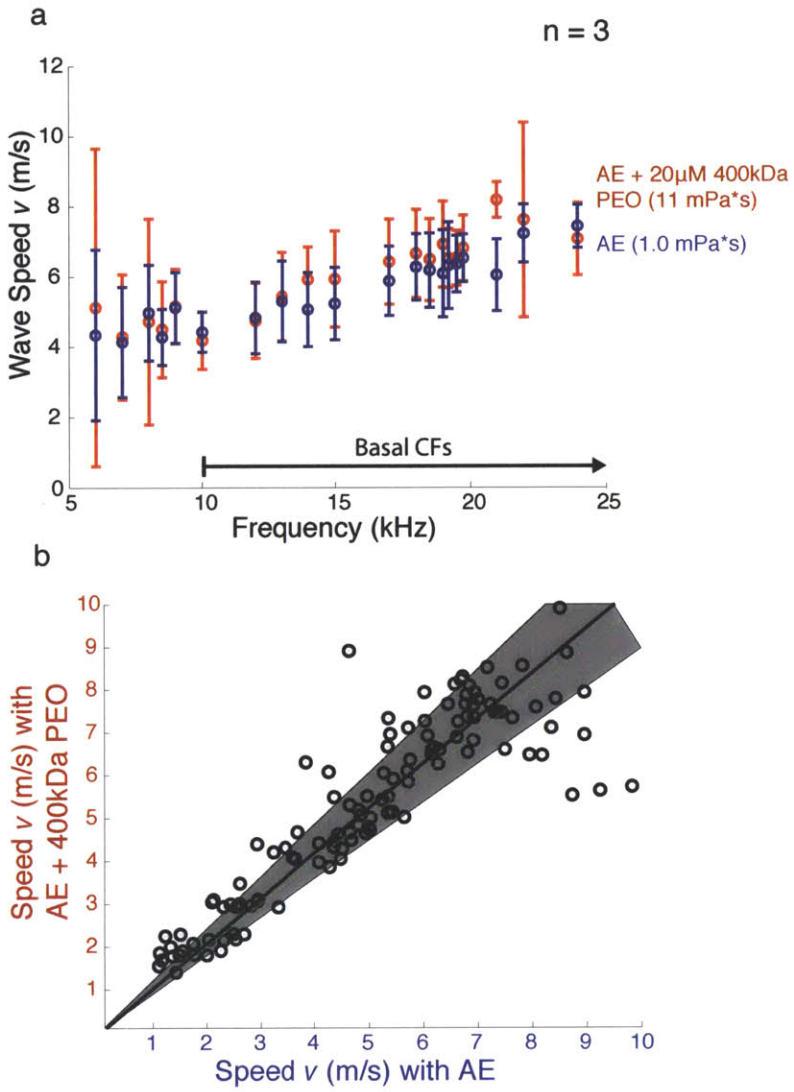

Figure 3-9: Propagation velocity of basal TM waves upon with increased external viscosity. Median wave velocities and interquartile ranges measured in TMs immersed in artificial endolymph (blue circles) and artificial endolymph with 10μm 400 kDa PEO (red circles) at variety of stimulus frequencies. (a) The median velocities for the TMs immersed in artificial endolymph with PEO were nearly identical (10.53 $\pm$ 1.96 m/s; n = 3 preparations) to those in just artificial endolymph (11.78 $\pm$ 2.20 m/s; n = 3 preparations). (b) Pairing the results with artificial endolymph speeds (x-axis) versus artificial endolymph (y-axis) also reveals no changes in speed. Median and interquartile ranges are indicated by black lines and shaded regions, respectively. ($\frac{v_{AE+PEG}}{v_{AE}} = 1.05 \pm 0.16$) Here it is clear that increasing the viscosity around the TM, rather than inside the TM has little impact on TM wave speed.

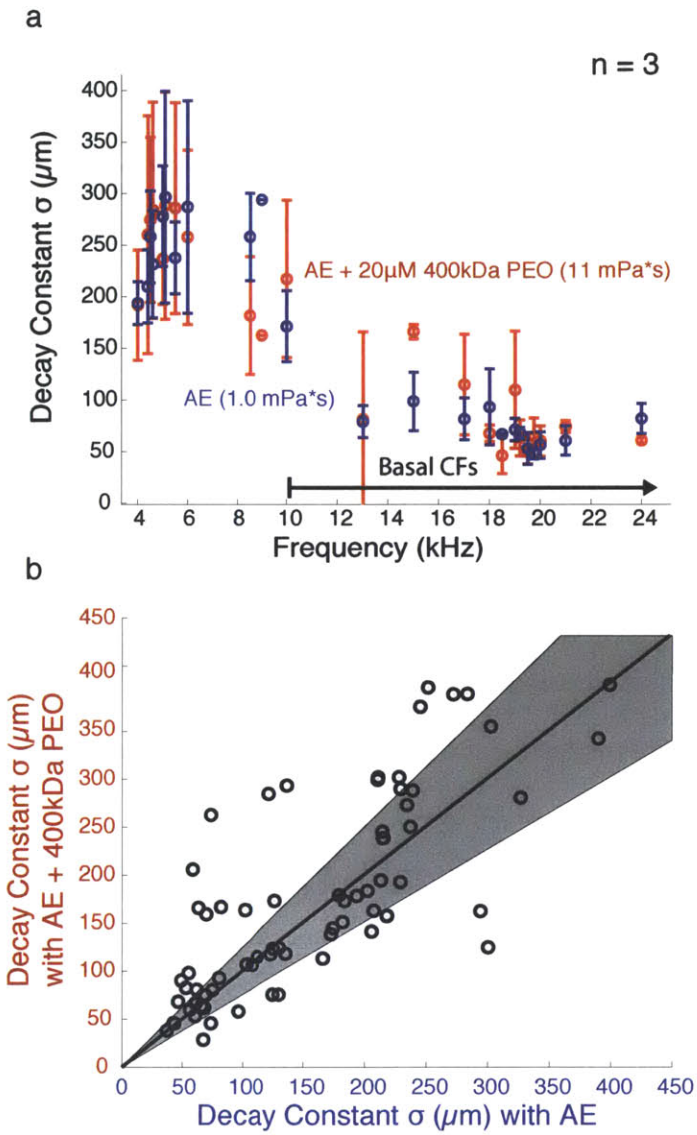

Figure 3-10: Wave decay constant calculation for basal TMs in artificial endolymph solutions with and without 10μm 400kDa PEO. (a) Wave decay constants versus stimulus frequency. TM segments in artificial endolymph (n = 5 preparations, blue circles) had median wave decay constant (σ) values of 137 $\pm$ 73 μm. Introducing 400kDa PEO to the artificial endolymph solution (n = 3 preparations, red circles) had little effect on decay constants as they displayed median decay constants of 157 $\pm$ 82 μm for the same frequency range. (b) Pairing the data reveals the same trend of no change in decay constant with increased external viscosity. Wave parameters plotted with artificial endolymph (x-axis) and artificial endolymph with 400kDa PEO (y-axis). Median and interquartile ranges are indicated by black lines and shaded regions, respectively ($\frac{\sigma_{AE+PEG}}{\sigma_{AE}} = 1.00 \pm 0.25$).

cannot propagate waves infinitely, a finite difference model was analyzed that consisted of a series of masses, longitudinally distributed, coupled to viscous and elastic elements. Best fits for these material properties for basal TMs (G' = 36±1.0 kPa, η = 0.20±0.05 Pa*s; n = 5 preparations) in artificial endolymph versus in artificial endolymph with PEG (G' = 33±5.5 kPa, η = 0.63±0.08 Pa*s; n = 5 preparations) revealed that adding PEG to the AE solution caused little change in shear storage modulus but increased shear viscosity by a factor of 3.15. Table 2 summarizes the material properties found. This result suggests that the changes in wave parameters seen here is completely due to changes in shear viscosity rather than shear storage modulus.

	G'	η
AE	36±1.0 kPa	0.20±0.05 Pa*s
AE + 20mM 8kDa PEG	33±5.5 kPa	0.63±0.08 Pa*s

Table 2: Material properties G' and η determined from wave results

3.3 Viscosity and TectB Mutant Mice

This section involves understanding how the wave results obtained under conditions of increased viscosity may relate to TM mutants. Many tectorial membrane mutations have been shown to reduce cochlear sensitivity [35, 26, 27]. For example, mutations in β-tectorin have been shown to decrease sensitivity dramatically in the apex [35] and decreases in traveling wave speeds have been demonstrated as a possible explanation for this change in sensitivity [15]. Work by Ghaffari et al. demonstrated that waves in the apical TM's of TectB mutant mice had properties suggesting a decrease in shear viscosity by half. Given this effect and that transmission electron micrographs imaging of apical TectB TM's have revealed that these mutant TM's appear to be more porous [35] and that changing the shear modulus of the TM had no impact on wave speed [9], there is a real possibility that pore size controls the speed of tectorial membrane waves and ultimately is the origin of changes in cochlear sensitivity seen in TectB mutant mice. To test this hypothesis, PEG of small molecular weight (8kDa,

20mM) was added to the bath surrounding the apical TectB mutant TMs and wave properties were assessed (figures 3-11, 3-12). Wave speeds of these TectB mutants increased back to their wild type values upon adding PEG to the artificial endolymph bath. This result suggests that porosity (and in turn, shear viscosity) of the TM is essential in controlling wave speed. Wave decay constants were also seen to drop below their initial values confirming that increasing shear viscosity has the property of decreasing decay constants.

3.4 Shear Impedance of the TM

3.4.1 Impedance of the TM and Intrinsic Viscosity

In addition to wave results, shear probe [19] measurements were conducted in the presence of PEG. Briefly, TM samples were extracted from the basal turn of mouse cochleae and placed onto a glass slide with Cell Tak (BD Biosciences Inc., Franklin Lakes, NJ). Using a microfabricated probe as seen in figure 2-2, forces were applied to the TM. Specifically, the square tip was lowered onto onto Hensen's stripe of the TM surface via a micromanipulator (Rucker and Kolls Inc., Milpitas, CA). The base of the probe was then stimulated radially with a piezo-electric actuator with frequencies from 1-80kHz. After acquisition of 16 evenly spaced phases, displacements of the base and tip of the probe were measured. From these, the impedance of the TM was determined:

$$Z_{TM}(\omega) = k_{mp}\frac{X_b(\omega) - X_p(\omega)}{j\omega X_p(\omega)} \tag{3.2}$$

where X_p is the probe tip displacement, X_b is the probe base displacement, and k_{mp} is the stiffness of the probe in the radial direction ($\sim$1.7 N/m). The artificial endolymph bath surrounding the TM was exchanged with artificial endolymph containing a variety of PEG concentrations with the same procedure described for TM wave measurements.

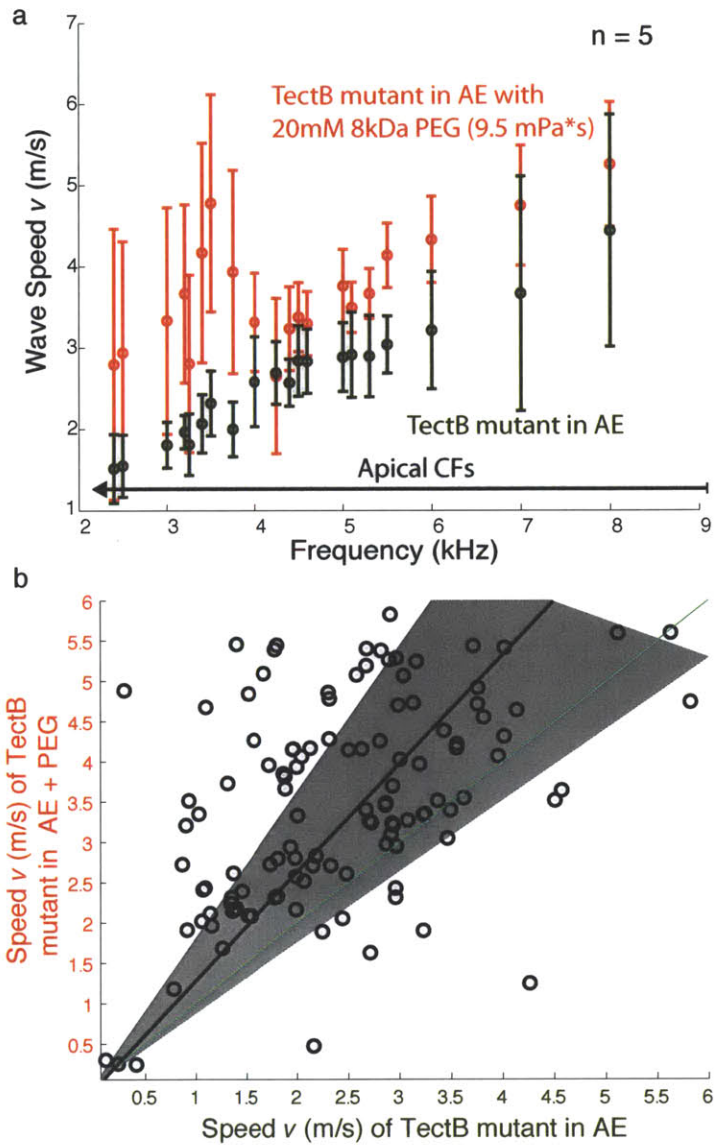

Figure 3-11: Propagation velocity of apical TM waves from TectB mutants upon increasing viscosity. Median wave velocities and interquartile ranges measured in TectB mutant TMs immersed in artificial endolymph (brown circles) and artificial endolymph with PEG (red circles) at variety of stimulus frequencies. (a) The median velocities for apical TectB mutant TMs immersed in artificial endolymph with PEG were higher (4.16 ± 1.45 m/s; n = 5 preparations) compared to those in just artificial endolymph (2.71 ± 0.99 m/s; n = 5 preparations). (b) Pairing the results with artificial endolymph speeds (x-axis) versus artificial endolymph with PEG (y-axis) also reveals the changes in speed as returning to near wild type upon increasing the intrinsic viscosity of the TM. Median and interquartile ranges are indicated by black lines and shaded regions, respectively. ($\frac{v_{AE+PEG}}{v_{AE}} = 1.35 \pm 0.47$)

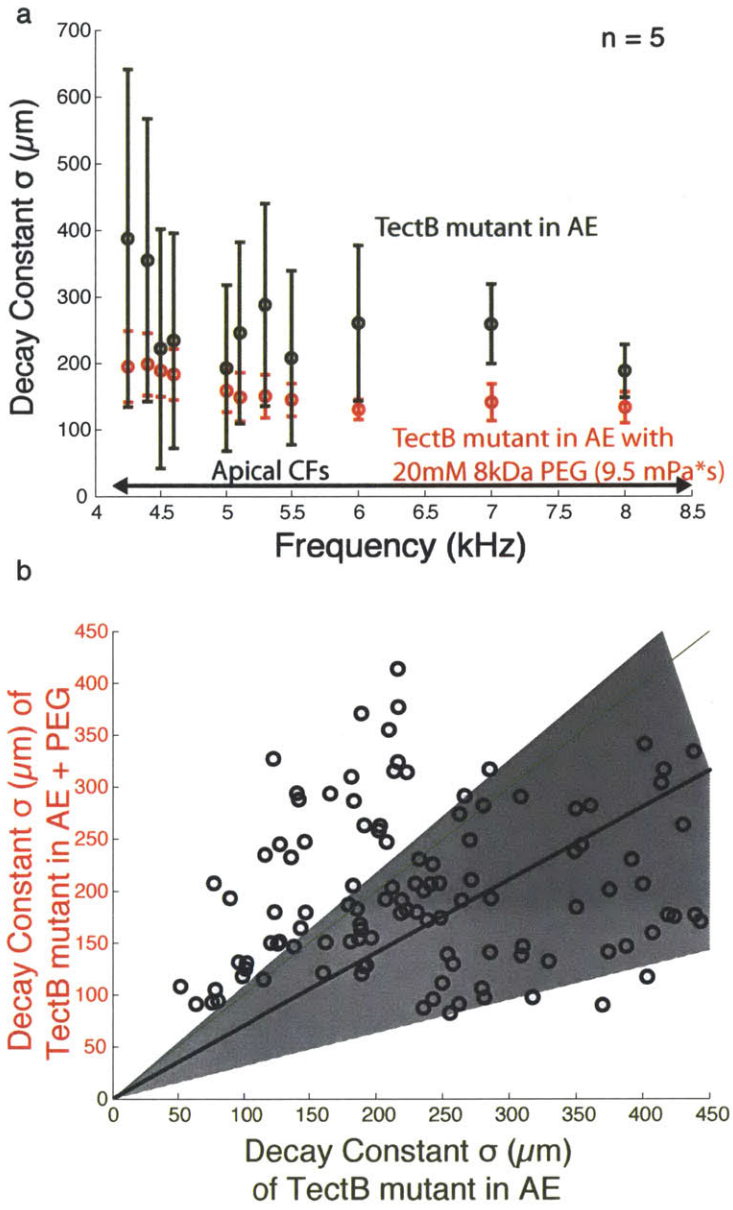

Figure 3-12: Wave decay constant calculation for apical TectB mutant TMs in artificial endolymph solutions with and without PEG. (a) Wave decay constants versus stimulus frequency. TectB mutant TM segments in artificial endolymph (n = 5 preparations, brown circles) had median wave decay constant (σ) values of 223 $\pm$ 67 μm. Introducing 8kDa PEG to the artificial endolymph solution (n = 5 preparations, red circles) had the effect of dropping these decay constants as they displayed median decay constants of 201 $\pm$ 58 μm for the same frequency range. (b) Pairing the data reveals the same trend of decreasing decay constant with increased viscosity for these TectB mutant TMs. Wave parameters plotted with artificial endolymph (x-axis) and artificial endolymph with PEG (y-axis) (n = 5). Median and interquartile ranges are indicated by black lines and shaded regions, respectively. ($\frac{\sigma_{AE+PEG}}{\sigma_{AE}} = 0.70 \pm 0.38$).

Results suggest that increasing intrinsic viscosity increases both the viscous and elastic moduli of the TM. However, it seems that the loss modulus changes more than the elastic modulus. Furthermore, after replacing the higher viscosity bath with artificial endolymph at physiological conditions (figure 3-14) it is clear that both the elastic and viscous moduli return approximately to their initial values. Furthermore, viscosity of the same TM was increased by adding PEG of various concentrations (3mM 8kDa (1.3mPa*s), 10mM 8kDa (3.4 mPa*s), and 20mM 8kDa (9.5mPa*s)) to the artificial endolymph bath (figure 3-15). Upon increasing viscosity linearly, linear increases in viscous and elastic moduli of the TM were seen.

3.4.2 Determining Material Properties from Shear Impedances

To understand the underlying material properties that give rise to the TM's dynamic nature, G' (shear stiffness) and η shear viscosity were determined from the shear impedance of the TM, Z_{TM} as follows:

$$G* = j\omega Z_{TM}\frac{1-\upsilon^2}{4r(1+\upsilon)} = G' + j\omega\eta \tag{3.3}$$

where υ is Poisson's ratio ($\sim$0.5 for audio frequencies) and r is the force probe's radius ($\sim 50\mu$m, which includes the moving surrounding tissue). Thus, examining the shear impedance obtained by analyzing the shear probe measurements, the resulting parameters calculated are G', the shear modulus, describes the tissue's stiffness, and η, the tissue's viscosity.

Figure 3-16 shows that by increasing the internal viscosity of the TM, G' (the TM's stiffness) increases by a small amount while η (the TM's viscosity) increased by a much larger factor. Specifically, η was 1.78x larger while G' was only 0.31x larger. By shearing the TM with the micro-fabricated probe (figure 2-2), the shearing parameters were measured through the TM body. Since TM properties are thought to be similar through bulk properties along the length of the TM, these parameters are relevant to TM waves and concur with the viscoelastic modeling (eq. 3.2) described earlier that

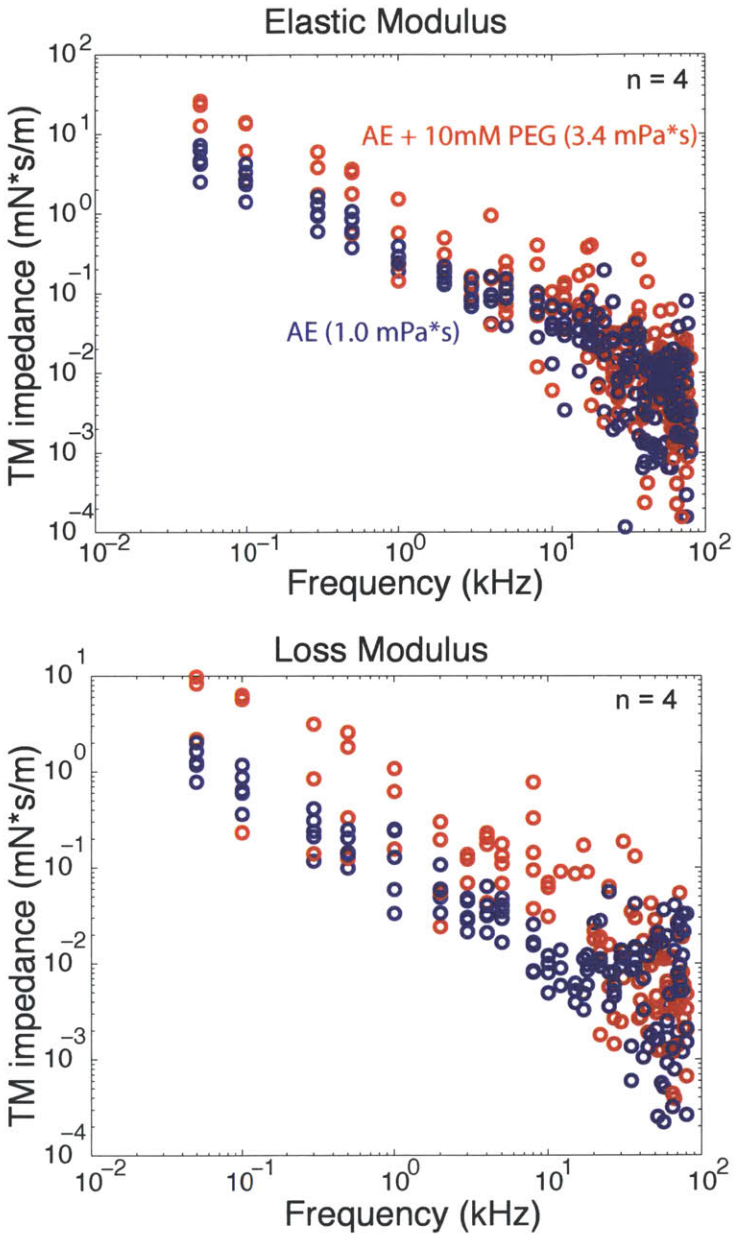

Figure 3-13: Bottom: Real component (loss modulus) at physiological conditions (blue) and after introducing 10mM 8kDa PEG to the solution (n = 4 preparations). Notice that there is a significant increase in loss modulus when increasing the intrinsic viscosity of the TM. Top: Imaginary component (elastic modulus) at physiological conditions and after introducing 10mM 8kDa PEG to the solution. Notice that there is an increase in elastic modulus when increasing the intrinsic viscosity of the TM, but the change is not as significant as with increases in viscous moduli.

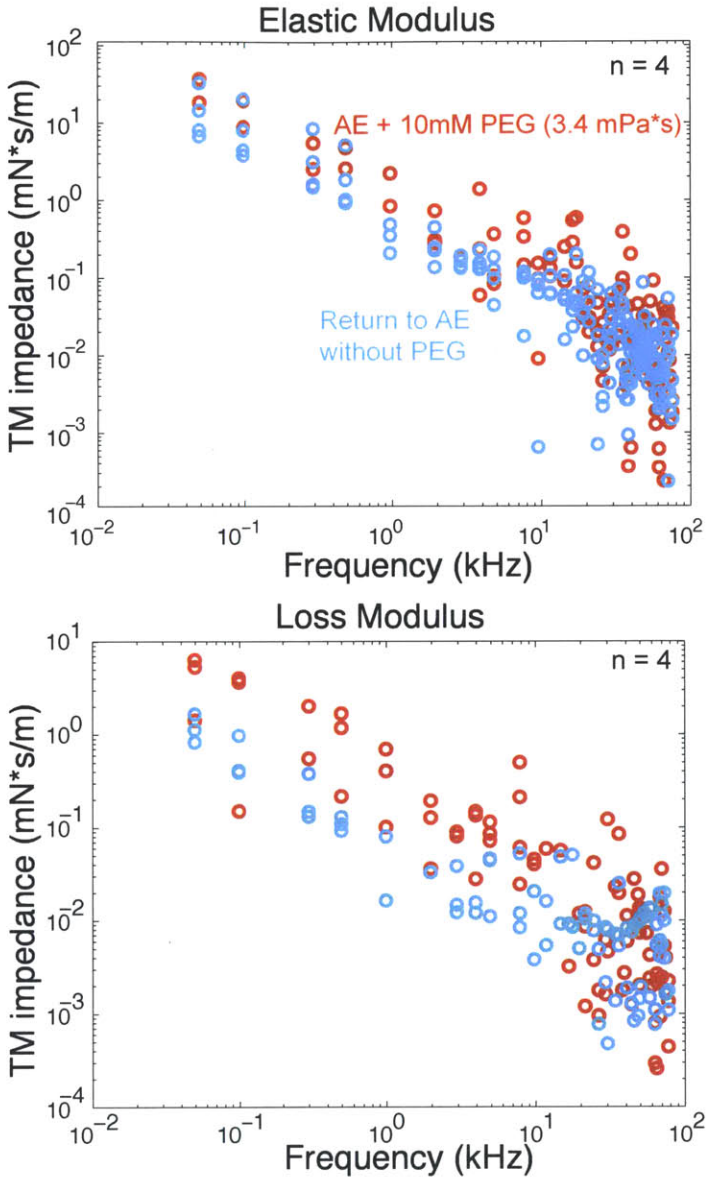

Figure 3-14: Real component (loss modulus, bottom)) and imaginary component (elastic modulus, top) upon increasing intrinsic viscosity with PEG (red) and after returning the solution around the TM back to physiological conditions (light blue). Notice that both the viscous and elastic moduli return to their values at physiological conditions when removing PEG from the artificial endolymph solution.

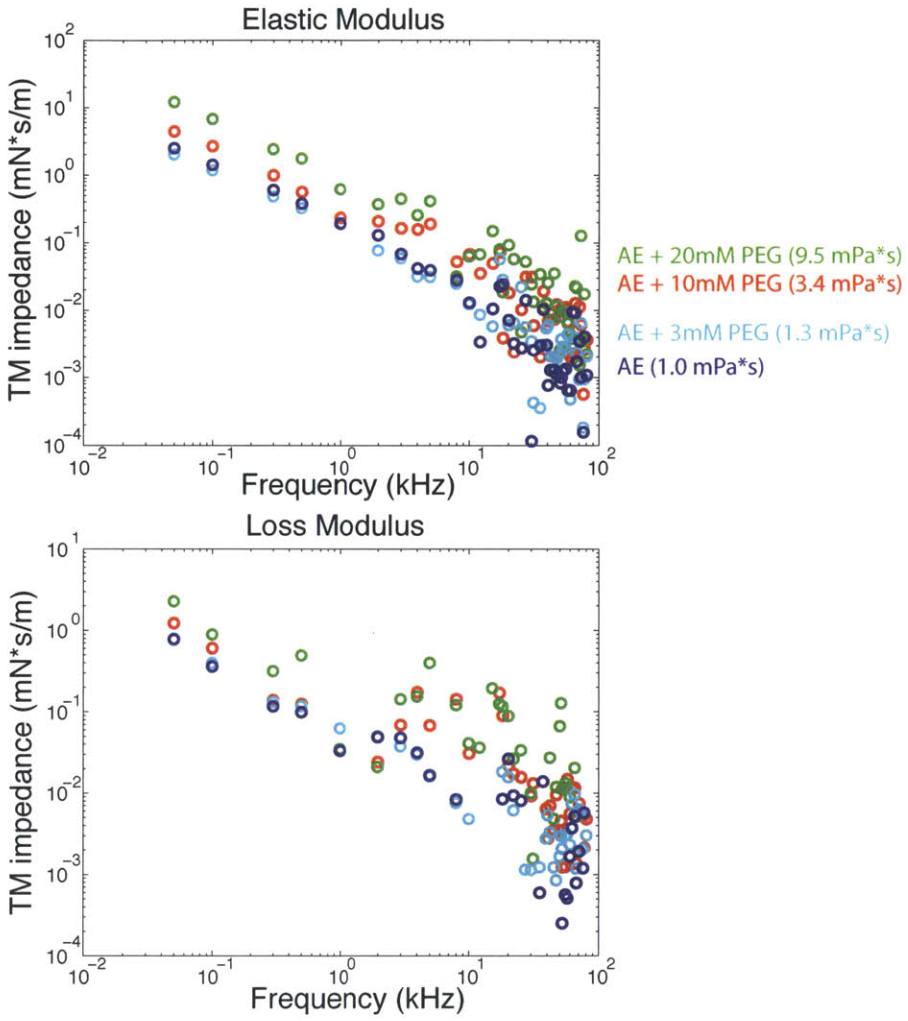

Figure 3-15: Real component (loss modulus, bottom) and imaginary component (elastic modulus, top) upon increasing intrinsic viscosity with several concentrations of 8kDa PEG (3mM, light blue; 10mM, red; 20mM, green). Notice that both viscous and elastic moduli increase upon increasing PEG concentration.

demonstrates shear viscosity (η) is the dominant parameter changed by introducing small molecular weight PEGs to the artificial endolymph bath surrounding the TM.

3.5 Viscoelastic Modeling of the TM

Viscoelastic Model of TM Wave Parameters

Given the material parameters extracted from wave measurements described in section 3.2 and from shear impedance measurements in section 3.4.2, a viscoelastic model of the TM was examined to determine if the results found agree with recent theory on TM mechanics. Furthermore, using such a model made it possible to predict TM wave parameters directly from the shear impedance measurements via the material parameters determined in section 3.4.2. To do so, a viscoelastic model relating material properties to wave parameters was used [16]. This model predicts and wave speed, ν and wave shear decay constant, σ, from shear modulus, G', and viscosity, η, as follows:

$$\sigma = \sqrt{\frac{2(G'^2 + \omega^2\eta^2)}{\rho\omega^2(\sqrt{G'^2 + \omega^2\eta^2} - G')}} \qquad v = \sqrt{\frac{2(G'^2 + \omega^2\eta^2)}{\rho(\sqrt{G'^2 + \omega^2\eta^2} + G')}} \tag{3.4}$$

where ρ is the density, and ω is the angular frequency ($\omega = 2\pi f$).

To understand how manipulating material parameters could impact TM waves, contour plots of decay constant (σ) and speed (ν) were examined as functions of shear modulus (G') and viscosity (η) at a variety of frequencies. Here, these contour plots are provided figure (figure 3-17) at frequencies of 20kHz and 7kHz. From these contour plots it can be inferred that changing shear viscosity, η, should have a large impact on speed and a smaller, but significant impact on decay constant, σ, especially at high frequencies. Also from these contour plots it is evident that shear modulus, G' should have the greatest impact on σ at all frequencies. To examine the effect of PEG on TM waves in context with this poroelastic model, values of G' and η found from the fitting the finite difference model to the wave data (3.2) obtained are drawn

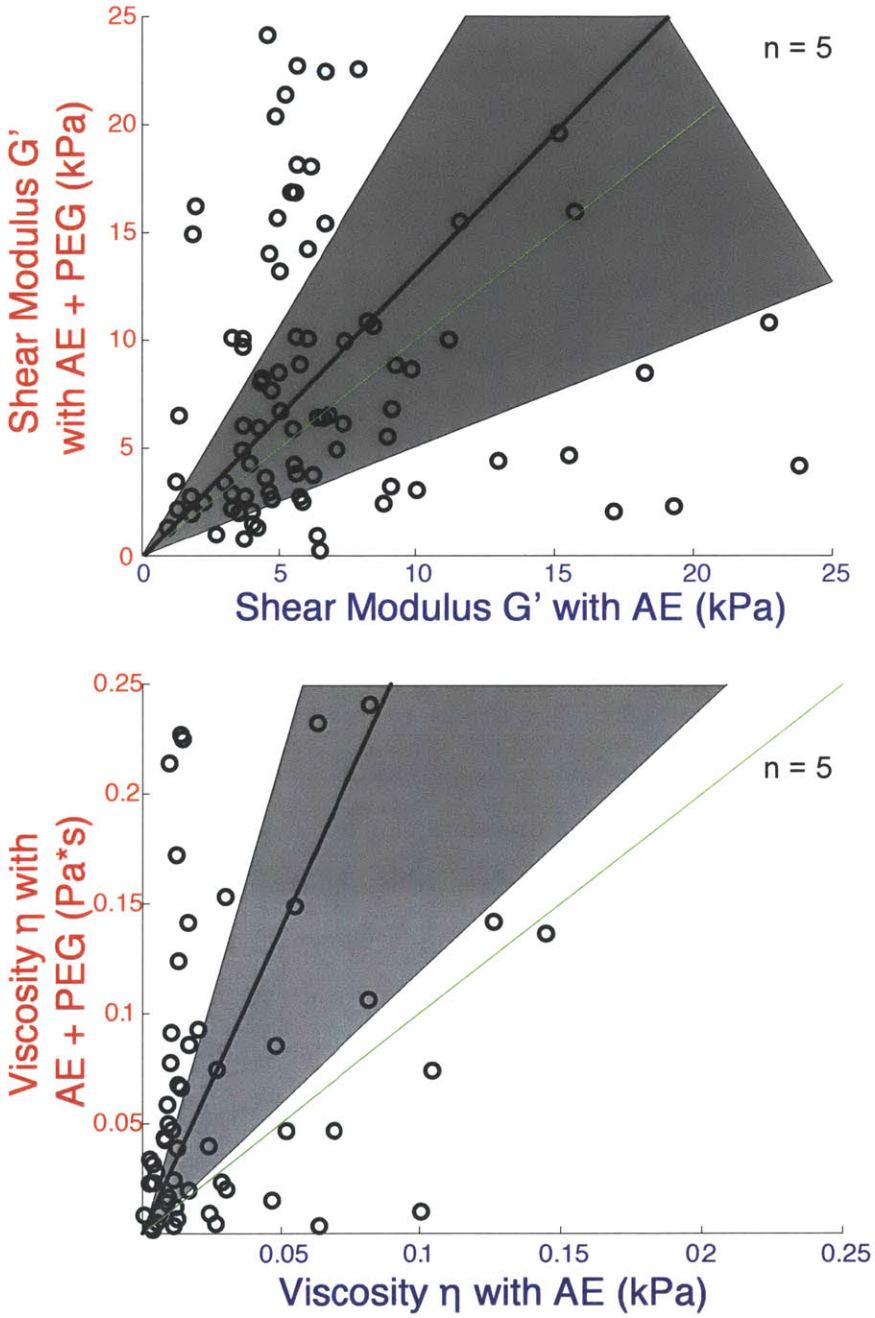

Figure 3-16: Material parameters determined from viscous and elastic moduli. Notice that while both viscosity η and shear modulus G' increase, η increases to a greater extent and the change is statistically more significant. Median and interquartile ranges are indicated by black lines and shaded regions, respectively ($\frac{\eta_{AE+PEG}}{\eta_{AE}} = 2.78 \pm 1.58$ $\frac{G'_{AE+PEG}}{G'_{AE}} = 1.31 \pm 0.81$).

as red (AE+PEG) and blue (AE alone) circles on the contour plots of figure 3-17. By looking at the values of G' and η estimated from the wave via the finite difference model it is evident that the wave speeds and decay constants found with and without the addition of PEG are accurately predicted by the viscoelastic model of waves.

3.5.1 Predicting Wave Parameters from Shear Probe Data via a Visco-Elastic Model of the TM

To verify the ability for shear probe data to predict TM wave measurements, TM wave parameters were calculated from the material parameters determined from shear impedance measurements (figure 3-16) using equation 3.4 to obtain the estimates for decay constant, σ, and speed, ν. Specifically, the material parameters determined in section 3.4.2 were used in conjunction with the viscoelastic model presented in the previous section. Figure (3-18) shows these results for material parameters extrapolated from five basal TM impedance measurements. These material parameters were determined from an independent measurement technique and introducing them to this viscoelastic wave model accurately predict the trends in wave decay and speed seen from direct TM wave measurements upon increases in shear viscosity via PEG. Thus, both the material parameters of the finite difference model examining TM waves and those extracted from shear impedance measurements accurately predict the wave speeds and decay constants seen here. Furthermore, this result confirms the finding that increasing shear viscosity has the effect of increasing both wave speed, ν, and decay constant, σ.

3.6 Electrokinetics and TM Pore Size

Mechanical strain is known to produce electrical responses [40] and electrical stimulation can also lead to mechanical deformations. This process is known as electrokinetics [17, 10]. Recently, it was reported that TM has an electrokinetic response due to the fixed charge of the membrane [13]. This phenomenon was demonstrated by applying

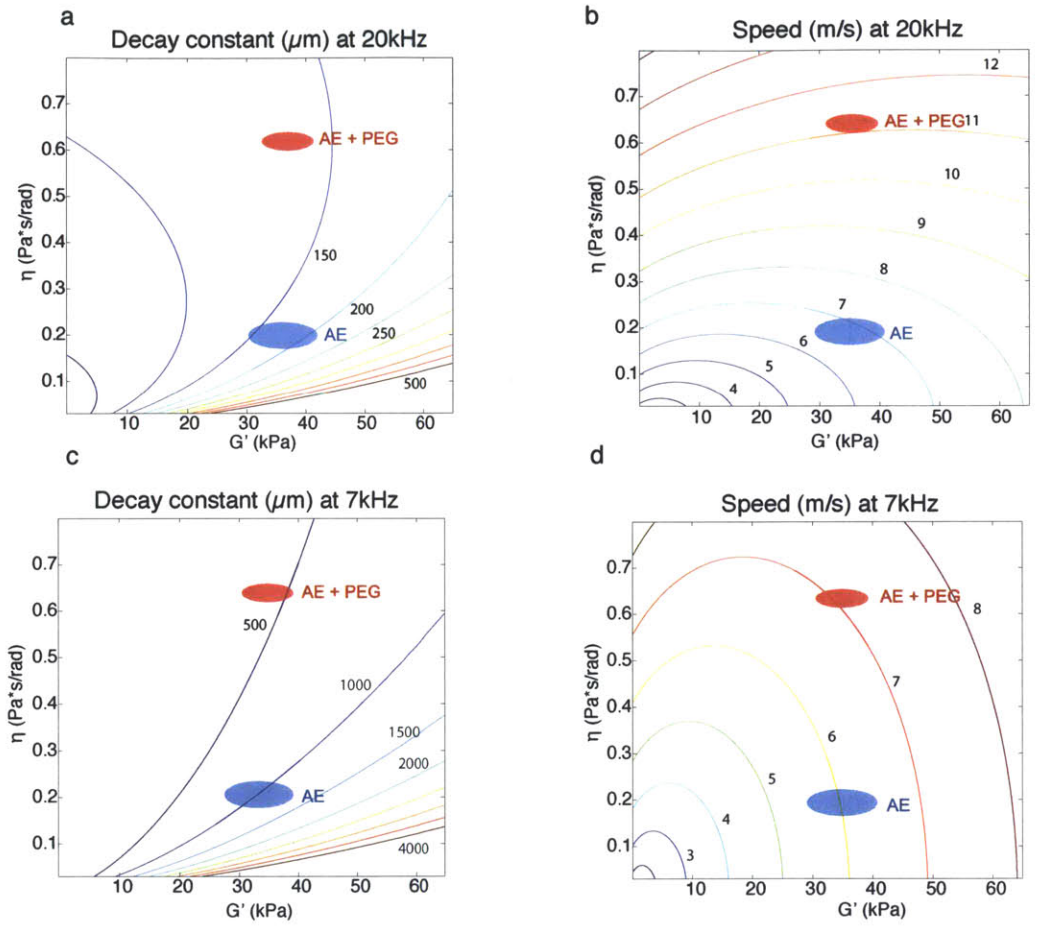

Figure 3-17: Viscoelastic model of TM wave parameters. (Left column) Contour plot of decay constant, σ, against viscosity, η, and shear storage modulus, G', at 7kHz (bottom) and 20kHz (top). (Right column) Contour plot of speed, ν, against viscosity, η, and shear storage modulus, G', at 7kHz (bottom) and 20kHz (top). Colored numbers on figures correspond to decay constant in μm or speed in m/s. Red circles indicate G' and η values calculated from fits to waves seen experimentally in artificial endolymph with PEG while blue circles indicate G' and η values calculated from waves at physiologic conditions.

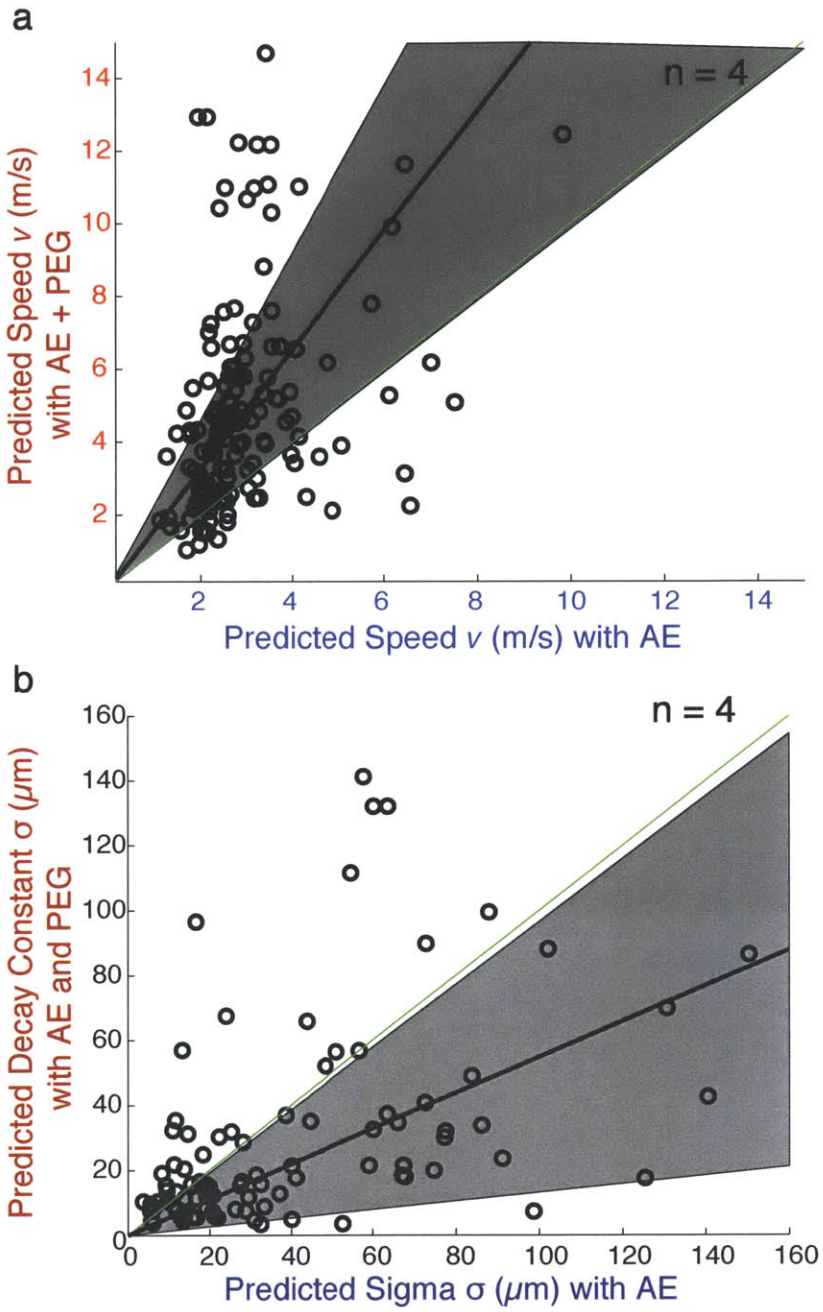

Figure 3-18: Wave parameters determined from material parameters determined from shear impedance experiments via a visco-elastic model of TM waves. Results from the previous figure were inputted into a viscoelastic model of waves to determine the expected effect on TM waves. Results suggest increases in speed accompanied with decreases in decay. These results confirm the TM waves measured in this thesis. Median and interquartile ranges are indicated by black lines and shaded regions, respectively ($\frac{v_{AE+PEG}}{v_{AE}} = 1.64 \pm 0.65$ $\frac{\sigma_{AE+PEG}}{\sigma_{AE}} = 0.55 \pm 0.42$)

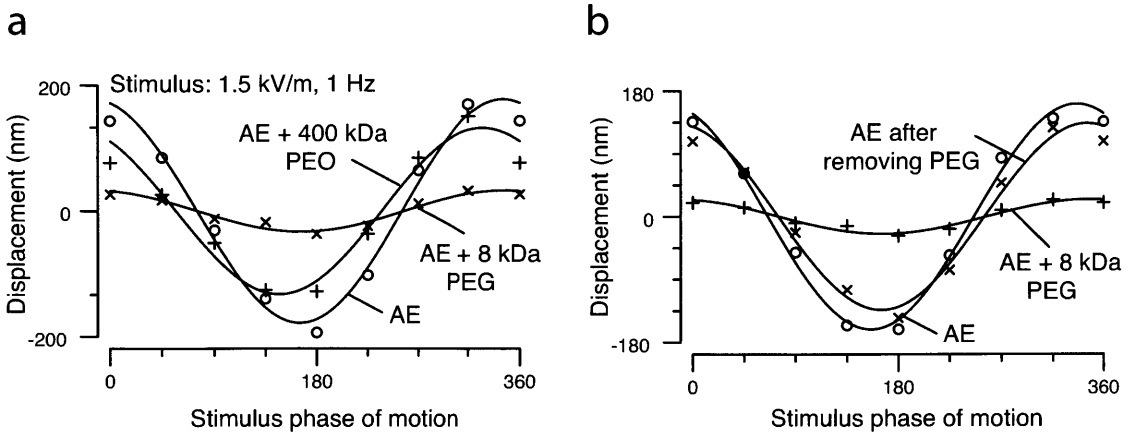

Figure 3-19: (a) Adding small PEG molecules (8 kDa, 3.4x increase in viscosity) to the AE solution resulted in a decrease in TM motion amplitude from 161 nm to 25 nm in response to a 1.5 kV/m, 1 Hz stimulus. In contrast, large PEG molecules (400 kDa, 4.5x increase in viscosity) resulted in much smaller changes (~20% reduction) in electrically-evoked motions of the TM. (b) Changes in TM motion caused by PEG were reversible. Returning the bath to AE without PEG caused TM motion to return the original magnitude.

oscillatory electric fields to the TM. Here, the effect of pore size on TM electrokinetics was evaluated by measuring TM motion in response to changes in both intrinsic and extrinsic viscosity. Internal viscosity of the TM was altered by adding small PEG molecules (10mM, 8 kDa) to the artificial endolymph solution. These were chosen because they had a radius of gyration small enough to enter the TM's nanopores [30]. To alter viscosity of the fluid surrounding the TM, AE with large PEO molecules (10 μM, 400 kDa) was used, which can not penetrate TM pores. Here, it was seen that adding small molecular weight PEGs decreased the TM's electrokinetic response at 1Hz by ~6.5x while adding large molecular weight PEO caused minor changes in TM motion despite the fact that the viscosities of the two solutions were the same (figure 3-19a). Furthermore, removing PEG from the solution caused the TM motions to return back to the original conditions observed (figure 3-19b).

Chapter 4

Discussion

Results in this study demonstrate the important nature of the TM's porous structure for controlling its mechanical properties. The porosity of the TM impacts its shear viscosity which is an essential material property controlling TM function. Here, it was seen that increasing the intrinsic viscosity of the TM with low molecular weight PEGs that could penetrate TM pores had the effect of increasing wave speed and decreasing wave decay constant. Analysis of a lumped parameter model of the TM showed that these changes in wave parameters can be explained by a change in shear viscosity with no accompanying change in shear modulus. Furthermore, analysis of a viscoelastic model of wave revealed the same changes in wave speed and decay seen experimentally with increases in shear viscosity. In contrast, introducing large molecular weight PEG has little effect on wave speed or decay, suggesting shear viscosity inside the TM plays a larger role in influencing the TMs mechanical properties than the surrounding fluid viscosity. This result suggests that fluid surrounding the TM has two separate effects on TM motion. First, increasing fluid viscosity has the obvious effect of increasing drag on the surface of the TM. In addition, if high viscosity fluid penetrates the TMs porous structure then the TMs material properties are also directly affected. Of these two effects, we see that the latter has a much greater impact on TM waves. Thus, the porosity of the TM may be critical to achieve the proper cochlear sensitivity and tuning.

4.1 TM Wave Speed and Sensitivity

Changes in TM wave velocity could have important implications for cochlear amplification. Cochlear amplification may arise from the interaction of two propagating waves, as described by Hubbard [20]. Specifically, Hubbard's model demonstrates that wave amplification arises when the velocities of two waves are matched. Since changing the intrinsic viscosity of the TM had the effect of increasing wave speed, the TM's shear viscosity may be carefully controlled to maintain appropriate sensitivity. Recent modeling work by Meaud and Grosh has shown that when tectorial membrane is longitudinally coupled and its shear viscosity is increased, cochlear sensitivity drops [31]. Given that changes in wave speed were observed here with changes in shear viscosity, it is possible that wave speed changes underly the changes in sensitivity observed. Since changing internal viscosity of the TM can be thought of as functionally equivalent to reducing TM pore size, the TM pore size may be tightly controlled to achieve the correct speeds necessary for proper cochlear amplification and ultimately proper cochlear sensitivity. Figure 4-1 describes the wave speed result observed in this thesis and connects the finding to Hubbard's two wave model and shear viscosity results from Meaud and Grosh's work.

4.2 Porosity, Sensitivity, and TectB Mutant Mice

Previously it was shown that apical TectB knockout TMs have a more porous structure [35] and that wave speed decreases [15]. By changing the internal viscosity of TectB mutant TMs, this experiment was functionally equivalent to reducing the pore size back to a condition that may more accurately represent the pore size of TMs from wild type mice. Given that speeds were seen to return back to wild-type velocities upon adding small molecular weight PEG to the AE bath surrounding TectB knockout TMs, pore size may control wave speed. Ultimately, these speed changes may influence cochlear sensitivity via a two wave model.

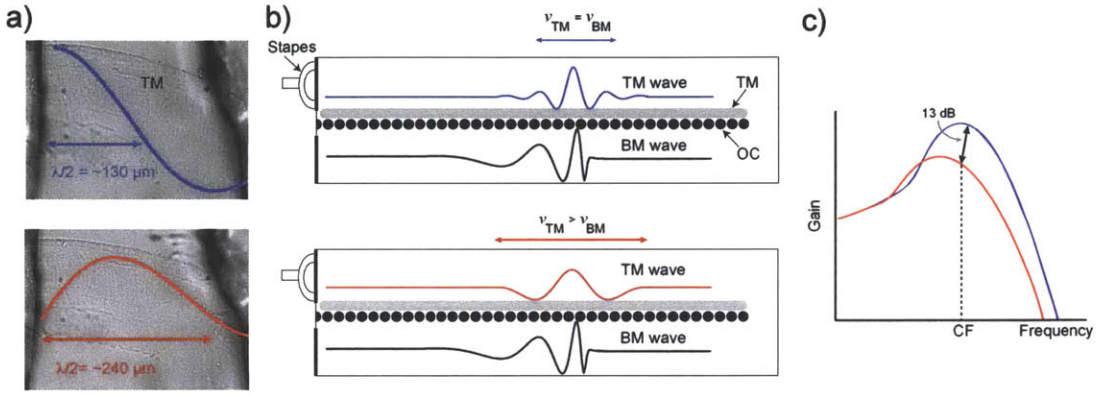

Figure 4-1: (a) Light microscope images of typical basal TM samples in the wave chamber with (bottom, red) and without PEG (top, blue). Superimposed waveforms illustrate TM wave displacements in response to 19 kHz stimulation in conditions with and without PEG. Fits to the data reveal that adding PEG to the bath increased the propagation wavelength ($\lambda/2 = \sim 130$ μm for the TM in AE (blue); $\lambda/2 = \sim 240$ μm for the TM in AE+20mM 8kDa PEG (red)). (b) Representation of two conditions in terms of a two wave model. With increased shear viscosity (red) the TM's wave speed would not match with the basilar membrane wave speed. Specifically, increasing intrinsic viscosity causes the wave length to increase. (c) Frequency tuning curves (adapted from Meaud and Grosh [31]) showing changes in sensitivity between a TM with typical shear modulus and shear viscosity parameters (blue line) and a TM with double the shear viscosity (red line). Arrow indicates the changes in sensitivity between these two conditions as approximately 13dB.

4.3 Shear Impedance Measurements

Results from the shear impedance measurements revealed that increasing intrinsic viscosity increases both the loss and elastic moduli of the TM. Furthermore, since returning the AE solution back to physiologic conditions caused both the elastic and loss moduli to revert to their original values, it can be inferred that the changes due to addition of PEG were due to changes in intrinsic viscosity rather than time dependent effects. One intriguing finding was that it seemed that the viscous modulus changes to a greater extent than the elastic modulus. The material properties (G' and η) determined from this data also predicted the same trend—both increased while η increased to a greater extent. Furthermore, calculating wave parameters via a viscoelastic model of TM waves with the material properties determined from these shear impedance experiments accurately predicted the changes seen in wave speed and decay. These results suggest that the shear impedance measures taken with increased intrinsic viscosity accurately account for the changes seen from the wave experiments. A question that remains is why both the elastic and viscous moduli changed for this experiment when distributed impedance analysis of the wave experiments revealed little to no change in shear storage modulus, G' compared to shear viscosity η. One possibility for this difference is that the shear probe entrained more springs due to viscous coupling.

4.4 Viscoelastic Modeling Confirms Wave Parameters Observed

Material parameters extracted from the wave measurements via a distributed impedance model revealed changes in η with little change in G'. The values obtained for G' and η for conditions with artificial endolymph and conditions with artificial endolymph with PEG were examined in terms of a viscoelastic model. From this comparison, it is evident that the wave speeds and decay constants found with and without the addition of PEG were accurately predicted by the viscoelastic model of waves at all

frequencies. This result suggests that a viscoelastic model is able to account for the changes in poroelastic mechanics that were probed with these experiments. A remaining question is why the viscoelastic model is able to predict these results well. One possibility is that the porosity of the TM is essential for maintaining the correct material properties (or in this case, letting PEG into the membrane). Once G' and η are established, the viscoelastic model is adequate to explain wave motions at audio frequencies. Next steps include examining poroelastic models of waves to see how the results found in this work align.

4.5 TM Pore Size and Electrokinetic Response

Previously, it has been shown that electrokinetic responses are influenced by changes in charge [13]. This work suggests that porosity is a critical component needed to achieve appropriate electrokinetic responses that act in tandem with charge in the tectorial membrane. By comparing changes to the internal viscosity (and in turn, the pore size) of the TM versus changes in viscosity of the surrounding fluid, this work revealed a strong dependence of TM electrokinetic interactions on porosity and a weak dependence on external viscosity of the surrounding fluid. Ultimately, these results provide a framework for a general poroelastic model of the TM under dynamic conditions. Thus, this work highlights the important interplay between fixed charge groups, porosity and the internal water content of the TM at the nanoscale.

Chapter 5

Conclusions

This thesis involved examining the effect of viscosity and pore size on the TMs dynamic processes that may play a critical role in achieving cochlear sensitivity and selectivity. It was discovered that the TM's intrinsic viscosity and pore size can influence phenomena such as waves and electrokinetics. The experiments included in this thesis demonstrate that:

(1) Adding low molecular weight PEG to the AE bath

- Increases TM wave speed
- Decreases TM wave decay constant
- Reduces electrokinetic responses of the TM
- Restores wild-type speeds to the TectB knockout TM

(2) Adding high molecular weight PEG to the bath has little effect on any of the previous properties

(3) These results fit with a simple model:

- Low molecular weight PEG permeates the porous structure of the TM while high molecular weight PEG is excluded
- When low molecular weight PEG permeates the TM it increases the loss modulus of the TM with little affect on shear modulus
- Changes in loss modulus are sufficient to
  - Increase TM wave speed

- Decrease wave decay constant
- Reduce electrokinetic responses

(4) Adding low, but not high, molecular weight PEG to the AE bath changes shear impedance measured with a micro-fabricated shearing probe. Specifically, the following are seen:

- Large increases in the viscous component
- Small increases in stiffness
- These shear impedance results suggest coupling limits interpretation of shear measurements as proportional to material properties and that the distributed impedance model more accurately reflects material properties determined.

The findings presented in this work reveal how the poroelastic properties of the TM can impact dynamic properties of the TM such as traveling waves and electrokinetics. Given these results, the porosity of the TM may have important implications for maintaining hearing properties. An important next step will be to connect these experimental results to a poroelastic model of the TM and ultimately a cochlear model. Doing so would help reveal how the motions observed here are relevant *in vivo* and ultimately how TM pore size and intrinsic viscosity play a role in maintaining proper cochlear sensitivity and selectivity. Ultimately, connecting the results conveyed in these *in vitro* experiments to a live cochlea or model would further demonstrate the importance of porosity on hearing.

Bibliography

[1] C.C. Abnet and D.M. Freeman. Deformations of the isolated mouse tectorial membrane produced by oscillatory forces. *Hear Res*, 144:29–46, 2000.

[2] J. B. Allen. Cochlear micromechanics — a physical model of transduction. *J Acoust Soc Am*, 68:1660–1670, 1980.

[3] W. E. Brownell, C. R. Bader, D. Bertrand, and Y. de Ribaupierre. Evoked mechanical responses of isolated cochlear hair cells. *Science*, 227:194–196, 1985.

[4] S. Chen, M. Fatemi, and J. F. Greenleaf. Quantifying elasticity and viscosity from measurement of shear wave speed dispersion. *J Acoust Soc Am*, 115:2781–2785, 2004.

[5] P. Dallos, M. C. Billone, J. D. Durrant, C. Wang, and S. Raynor. Cochlear inner and outer hair cells: functional differences. *Science*, 177:356–358, 1972.

[6] C. Q. Davis and D. M. Freeman. Statistics of subpixel registration algorithms based on spatio-temporal gradients or block matching. *Optical Engineering*, 37:1290–1298, 1998.

[7] C. Q. Davis and D. M. Freeman. Using a light microscope to measure motions with nanometer accuracy. *Optical Engineering*, 37:1299–1304, 1998.

[8] H. Davis. Biophysics and physiology of the inner ear. *Physiol Rev*, 37:1–49, 1957.

[9] S. Farrahi, R. Ghaffari, and D. M. Freeman. pH alters decay but not speed of tectorial membrane waves. In *Mechanics of Hearing Conference*, July 2011.

[10] E. H. Frank and A. J. Grodzinsky. Cartilage electromechanics– i. electrokinetic transduction and the effects of electrolyte ph and ionic strength. *J. Biomechanics*, 20:615–627, 1987.

[11] D. M. Freeman, D. A. Ehsani, and T. F. Weiss. The osmotic response of the isolated tectorial membrane of the chick to isosmotic solutions: Effect of (Na^+), (K^+), and (Ca^{2+}) concentration. *Hearing Res.*, 79:197–215, 1994.

[12] D.M. Freeman, K. Masaki, A.R. McAllister, J.L. Wei, and T.F. Weiss. Static material properties of the tectorial membrane: a summary. *Hear Res*, 180:11–27, 2003.

[13] R. Ghaffari. The functional role of the mammalian tectorial membrane in cochlear mechanics. *PhD Thesis. MIT, Cambridge, MA*, 2008.

[14] R. Ghaffari, A. J. Aranyosi, and D. M. Freeman. Longitudinally propagating traveling waves of the mammalian tectorial membrane. *Proc Nat Acad Sci USA*, 104:16510–16515, 2007.

[15] R. Ghaffari, A. J. Aranyosi, G. P. Richardson, and D. M. Freeman. Tectorial membrane traveling waves underlie abnormal hearing in tectb mutants. *Nature Communications*, 1, 2010.

[16] J. F. Greenleaf, M. Fatemi, and M. Insana. Selected methods for imaging elastic properties of biological tissues. *Ann Rev Biomed Eng*, 91:57–78, 2003.

[17] A. J. Grodzinsky. Electromechanical and physicochemical properties of connective tissue. *CRC Critical Rev In Biomed Engin*, 9:133–199, 1983.

[18] J. W. Gu, W. Hemmert, D. M. Freeman, and A. J. Aranyosi. Frequency-dependent shear impedance of the tectorial membrane. *Biophys. J.*, 91:2356–70, 2008.

[19] J. W. Gu, W. Hemmert, D. M. Freeman, and A. J. Aranyosi. Frequency-dependent shear impedance of the tectorial membrane. *Biophys J*, 95:2529–38, 2008.

[20] A. E. Hubbard. A traveling-wave amplifier model of the cochlea. *Science*, 259:68–71, 1993.

[21] A. J. Hudspeth. How the ear's works work. *Nature*, 341:397–404, 1989.

[22] H.J. Kennedy, A.C. Crawford, and R. Fettiplace. Force generation by mammalian hair bundles supports a role in cochlear amplification. *Nature*, 433:880–883, 2005.

[23] A. Kronester-Frei. Sodium dependent shrinking properties of the tectorial membrane. *Scanning Electron Microscopy*, 2, 1978a.

[24] A. Kronester-Frei. Sodium dependent shrinking properties of the tectorial membrane. *Scanning Elecron Microscopy*, 2:943–948, 1978b.

[25] A. Kronester-Frei. Localization of the marginal zone of the tectorial membrane in situ, unifixed, and with in vivo-like millieu. *Arch. Otorhinolaryngol.*, pages 224, 3–9, 1979.

[26] P. K. Legan, V. A. Lukashkina, R. J. Goodyear, A. N. Lukashkin, K. Verhoeven, G. V. Camp, I. J. Russell, and G. P. Richardson. A deafness mutation isolates a second role for the tectorial membrane in hearing. *Nature Neuroscience*, 8:1035–1042, 2005.

[27] P.K. Legan, V.A. Lukashkina, R.J. Goodyear, M. Kössl, I.J. Russell, and G.P. Richardson. A targeted deletion in α-tectorin reveals that the tectorial membrane is required for the gain and timing of cochlear feedback. *Neuron*, 28:273–285, 2000.

[28] D. Lim. Fine morphology of the tectorial membrane. *Arch. Otolaryngology*, 96:199–215, 1972.

[29] F Mammano and R Nobili. Biophysics of the cochlea: linear approximation. *J Acoust Soc Am*, 93:3320–3332, 1993.

[30] K. Masaki, T. F. Weiss, and D. M. Freeman. Poroelastic bulk properties of the tectorial membrane measured with osmotic stress. *Biophys. J.*, 91:2356–2370, 2006.

[31] J Meaud and K Grosh. The effect of tectorial membrane and basilar membrane longitudinal coupling in cochlear mechanics. *J Acoust Soc Am*, 127(3):1411–1421, Mar 2010.

[32] S. T. Neely and D. O. Kim. An active cochlear model showing sharp tuning and high sensitivity. *Hear Res*, 9:123–130, 1983.

[33] S. T. Neely and D. O. Kim. A model for active elements in cochlear biomechanics. *J Acoust Soc Am*, 79:1472–1480, 1986.

[34] G. P. Richardson, J. B. de Monvel, and C. Petit. How the genetics of deafness illuminates auditory physiology. *Annu. Rev. Physiol.*, 73:311–34, 2010.

[35] I. J. Russell, P. K. Legan, V. A. Lukashkina, A. N. Lukashkin, R. J. Goodyear, and G. P. Richardson. Sharpened cochlear tuning in a mouse with a genetically modified tectorial membrane. *Nature Neurosci*, 10:215–223, 2007.

[36] J. R. Sachs and A. J. Grodzinsky. An electromechanically coupled poroelastic medium driven by an applied electric current: surface detection of bulk material properties. *Physicochemical Hydrodynamics*, 11:585–614, 1989.

[37] D. Shah, D. M. Freeman, and T. F. Weiss. The osmotic response of the isolated, unfixed mouse tectorial membrane to isosmotic solutions: Effect of (Na^+), (K^+), and (Ca^{2+}) concentration. *Hearing Res.*, 87:187–207, 1995.

[38] S. J. Timoner and D. M. Freeman. Multi-image gradient-based algorithms for motion estimation. *Optical Engineering*, 40:2003–2016, 2001.

[39] A. Xia, S. S. Gao, T. Yuan, A. Osborn, A. Bress, M. Pfister, S. M. Maricich, F. A. Pereira, and J. S. Oghalai. Deficient forward transduction and enhanced reverse transduction in the alpha tectorin c1509g human hearing loss mutation. *Dis Model Mech*, 3:209–223, 2010.

[40] A. J. Grodzinsky Y.J. Kim, L.J. Bonasser. The role of cartilage streaming potential, fluid flow, and pressure in the stimulation of chondrocyte biosynthesis during dynamic compression. *J Biomech*, pages 1055–1066, 1995.

[41] J. J. Zwislocki. Tectorial membrane: a possible sharpening effect on the frequency analysis in the cochlea. *Acta Otolaryngol*, 87:267–269, 1979.

[42] J J Zwislocki. Five decades of research on cochlear mechanics. *J Acoust Soc Am*, 67(5):1679–1685, May 1980.